Chapter 4

Chemostratigraphy and the Neoproterozoic glaciations

GALEN P. HALVERSON[1,3]* & GRAHAM SHIELDS-ZHOU[2]

[1]*School of Earth and Environmental Sciences, The University of Adelaide, North Terrace, Adelaide, SA 5005, Australia*

[2]*Department of Earth Sciences, University College London, Gower Street, London, WD1E 6BT, UK*

[3]*Present address: Department of Earth and Planetary Sciences, McGill University, 3450 University Street, Montreal, QC, H3A 2A7, Canada*

**Corresponding author (e-mail: galen.halverson@mcgill.ca)*

Abstract: Although the pre-glacial Proterozoic isotopic record is poorly constrained, it is apparent that the chemical and isotopic composition of the oceans began to change during the early to mid-Neoproterozoic and experienced considerable fluctuations alongside climatic instability during much of the subsequent Cryogenian and Ediacaran periods. The earliest known large negative $\delta^{13}C$ excursion appears to post-date 811 Ma and fluctuations became progressively more extreme, culminating in the late-Ediacaran 'Shuram–Wonoka' anomaly. The negative excursions are commonly associated with pre-glacial and post-glacial times, while extremely high $\delta^{13}C$ values are characteristic of strata between glaciations. The precise causal mechanism for these excursions is subject to debate. Seawater $^{87}Sr/^{86}Sr$ rose during the Neoproterozoic, with abrupt increases following deglaciation consistent with enhanced weathering rates. Reported marine sulphate and pyrite $\delta^{34}S$ data exhibit marked variation through this interval, although the changes are not always consistent within or between sedimentary successions of equivalent age. Iron-speciation studies indicate that much of this variation was caused by fluctuating and low sulphate concentrations in seawater, which at times led to the build-up of ferruginous conditions in the ocean. The application of chemostratigraphy to understanding and correlating the Neoproterozoic glaciations evokes considerable controversy, and many questions persist regarding the reliability and calibration of the $\delta^{13}C$, $^{87}Sr/^{86}Sr$ and $\delta^{34}S$ record. Nevertheless, the individual glaciations appear to be characterized by distinct combined chemostratigraphic signatures, in large part due to the generally increasing strontium isotope composition of seawater through the Neoproterozoic Era.

Chemical stratigraphy has enjoyed widespread application to the study of the Neoproterozoic sedimentary record, in particular with regard to the number, correlation, causes and consequences of glaciations during this era. Owing to the scarcity of biostratigraphically useful fossils, it has become the tool of choice for global stratigraphic correlation of Neoproterozoic strata (Kaufman & Knoll 1995; Walter *et al.* 2000). In their broad survey of carbonates, Schidlowski *et al.* (1975) pioneered the application of carbon-isotope stratigraphy to the Precambrian sedimentary record. Williams (1979) subsequently documented negative $\delta^{13}C$ signatures associated with post-glacial carbonates in Australia. Knoll *et al.* (1986) later focused attention on the Neoproterozoic Era with coupled carbonate ($\delta^{13}C_{carb}$) and total organic carbon ($\delta^{13}C_{org}$) carbon-isotope records from carbonate-dominated successions in Svalbard and East Greenland that showed large and in-phase variations ostensibly linked to glacial episodes. This study complemented contemporaneous investigations that similarly showed large fluctuations in the $\delta^{13}C$ composition of ancient marine carbonates spanning the Precambrian–Cambrian boundary (Hsu *et al.* 1985; Tucker 1986; Magaritz *et al.* 1986). These studies bolstered the argument that ancient carbonates and sedimentary organic matter could be used as proxies for the carbon-isotopic composition of the seawater in which they formed. Inasmuch, they opened the door to carbon-isotope chemostratigraphy as a commonplace tool for basin- and global-scale correlation and as a measure of the behaviour of the exogenic carbon cycle, in particular as it related to extreme climate variability and biospheric change (e.g. Derry *et al.* 1992; Kaufman & Knoll 1995).

Notwithstanding challenges to the integrity of carbon-isotope signatures as proxies for seawater composition (e.g. Frimmel 2009; Knauth & Kennedy 2009; Derry 2010) and poor radiometric age control on many Neoproterozoic successions, carbon-isotope stratigraphy is a powerful tool for establishing a chronological framework for this interval, during which extensive carbonates were deposited but for which biostratigraphy is of limited (but increasing) use (Knoll & Walter 1992; Knoll 2000). Multiple negative carbon-isotope excursions and intervening intervals of sustained high $\delta^{13}C_{carb}$ appear to correlate globally (e.g. Kaufman *et al.* 1997; Halverson *et al.* 2005). However, because there are also multiple glaciations, each apparently associated with negative carbon-isotope anomalies, these excursions are non-unique and robust correlations, in the absence of firm radiometric ages, require additional data.

Like carbon isotopes, sulphur-isotope data on both pyrite and sulphate show impressive variability spanning the Neoproterozoic glaciations (Gorjan *et al.* 2000; Hurtgen *et al.* 2002). However, the strontium-isotope record is the most useful in discriminating between the various negative carbon-isotope anomalies because $^{87}Sr/^{86}Sr$ increases throughout most of the Neoproterozoic (Shields 1999; Melezhik *et al.* 2001; Halverson *et al.* 2007) such that each of the prominent carbon-isotope anomalies appears to be associated with distinct strontium-isotope signatures.

Many other chemostratigraphic methods have been applied to the Neoproterozoic sedimentary record. Iron speciation data have revealed remarkable fluctuations in the redox state of seawater throughout the Neoproterozoic, in particular spanning glaciations and leading up to the first appearance of the Ediacaran fauna (Canfield *et al.* 2007, 2008). Post-glacial carbonates have also proven to be exceptional archives of the highly unusual environmental conditions during recovery from the Cryogenian glaciations, preserving in some cases extraordinary geochemical anomalies in non-traditional geochemical proxies, such as calcium and boron isotopes (Kasemann *et al.* 2005) and $\Delta^{17}O$ (Bao *et al.* 2008). For a more extensive review of these and other chemostratigraphic methods applied to the Neoproterozoic sedimentary record, the reader is referred to Halverson *et al.* (2010). A detailed account of the application of the chemical index of alteration (CIA) to the Neoproterozoic glacial record is presented in this volume by Bahlburg & Dobrzinski (2011), and chemostratigraphic and geochronological data from individual sedimentary successions are summarized in reviews throughout

From: Arnaud, E., Halverson, G. P. & Shields-Zhou, G. (eds) *The Geological Record of Neoproterozoic Glaciations*. Geological Society, London, Memoirs, **36**, 51–66. 0435-4052/11/$15.00 © The Geological Society of London 2011. DOI: 10.1144/M36.4

this volume. The aim of this chapter is to provide a brief review of the carbon-, sulphur- and strontium-isotope systems and the iron-speciation proxy and a synthesis of published data bracketing the Neoproterozoic glaciations, with a focus on the structure of these records and their temporal relation to glaciation.

Carbon isotopes

Under normal conditions and at the scale of resolution appropriate in Precambrian chemostratigraphy, the carbon-isotope compositions of unaltered marine carbonates ($\delta^{13}C_{carb}$) precipitated in equilibrium with seawater closely approximate the composition of the total dissolved inorganic carbon (DIC) pool (Hayes *et al.* 1999). If it is assumed that the carbonates retain their primary signatures after burial, then carbon-isotope chemostratigraphy has diverse applications, such as establishing global correlations (e.g. Kaufman *et al.* 1993, 1997), regional studies of basin architecture and carbonate sequence stratigraphy (Halverson *et al.* 2002; Cozzi *et al.* 2004; Jiang *et al.* 2007), modelling of the global carbon cycle (Derry *et al.* 1992), and as a constraint on mechanisms for the causes of Neoproterozoic glaciation (Kaufman *et al.* 1997; Halverson *et al.* 2002; Schrag *et al.* 2002) and post-glacial carbonate deposition (Kaufman *et al.* 1997; Hoffman *et al.* 1998; Kennedy *et al.* 2001; Higgins & Schrag 2003; Shields 2005). Debate continues as to whether Neoproterozoic marine carbonates faithfully preserve their primary depositional signatures, particularly where they are highly ^{13}C-depleted (Bristow & Kennedy 2008; Frimmel 2009; Knauth & Kennedy 2009; Derry 2010). Nevertheless, the general consensus is that, by and large, ancient marine carbonates do preserve seawater compositions, so secular trends in $\delta^{13}C_{carb}$ can be interpreted in terms of inputs of carbon to and outputs from the global ocean (Holser 1997).

The record of the carbon-isotope composition of sedimentary organic matter ($\delta^{13}C_{org}$), while much less applied in the Neoproterozoic, is often used where carbonates are not sufficiently abundant to construct a $\delta^{13}C_{carb}$ profile. The analysis of $\delta^{13}C_{org}$ has recently surged due to the hypothesis that some of the extreme negative $\delta^{13}C_{carb}$ anomalies might be the result of partial oxidation of an enormous reactive organic carbon reservoir in the deep ocean (Rothman *et al.* 2003). Organic carbon data are intrinsically more difficult to acquire than inorganic carbon data, and the connection between extant kerogen (or total organic carbon, TOC) and original biomass is inevitably blurred by diagenesis, thermal alteration of the organic matter (Hayes *et al.* 1983; Kaufman *et al.* 1991; Hayes *et al.* 1999) and input of detrital kerogen. Nevertheless, early stratigraphically constrained Neoproterozoic $\delta^{13}C_{org}$ data sets (e.g. Knoll *et al.* 1986; Kaufman *et al.* 1997) showed broad correlation with contemporaneous $\delta^{13}C_{carb}$, suggesting that it could be used in parallel with or in place of (where primary carbonates are unavailable) inorganic carbon data as a proxy for seawater compositions, albeit with the caveat that the net fractionation between the original DIC reservoir and extracted kerogen is inherently variable. A compilation of organic carbon data by Hayes *et al.* (1999) suggested an average difference between contemporaneous carbonates and organic matter (ε_{TOC}) of *c.* 30‰ in the Neoproterozoic, but with large fluctuations ($\pm$10‰) associated with $\delta^{13}C_{carb}$ anomalies, in particular those spanning glaciations.

More recent and detailed data sets from Ediacaran-aged sediments have revealed sustained intervals where $\delta^{13}C_{carb}$ and $\delta^{13}C_{org}$ are decoupled or even anti-correlated (Calver 2000; Fike *et al.* 2006; McFadden *et al.* 2008). Swanson-Hysell *et al.* (2010) recently argued, based on new, paired data from Australia, that decoupling of these two proxies began sometime in the Cryogenian. Decoupling between these two proxies is a prediction of the Rothman *et al.* (2003) hypothesis, because the implied oceanic organic-carbon reservoir would be much larger than the DIC reservoir. While questions remain as to the plausibility of sufficient oxidants being available to generate the accompanying highly negative $\delta^{13}C_{carb}$ anomalies (Bristow & Kennedy 2008), the undeniable lack of correlation in certain data sets requires a mechanistic explanation.

Sulphur isotopes

Sedimentary sulphur-isotope ratios are measured on sedimentary sulphates or sulphides. Sulphur-isotope data on sulphates can be recovered, with varying degrees of reliability, from evaporites, barite, phosphorites and carbonates (as carbonate-associated sulphate, CAS). Sulphate-bearing marine minerals commonly do not form in isotopic equilibrium with seawater, so additional arguments need to be marshalled to support the presumption that they record seawater sulphate isotopic compositions. The $\delta^{34}S$ values of marine evaporite minerals may be higher or lower than contemporaneous seawater depending on the extent of basin restriction and connection to meteoric influence. Stratiform barite $\delta^{34}S$ values are also prone to deviate from seawater, although lowermost values are generally close approximations to ocean composition (Shields 2007). Phosphorite can also show higher $\delta^{34}S$ values than seawater due to Rayleigh fractionation during bacterial sulphate reduction (e.g. Hough *et al.* 2006), and the same may also be true of some diagenetic carbonate rocks (e.g. Marenco *et al.* 2008*a*). An additional problem with carbonate- (and phosphate-) associated sulphate sulphur-isotopic analyses derives from the inadvertent incorporation of contaminant sulphate during the dissolution process before analysis (Marenco *et al.* 2008*b*).

Unlike marine sulphate minerals, sulphides (typically pyrite) record the net fractionation imparted during bacterial sulphate reduction (BSR), plus additional fractionation effects contributed by disproportionation reactions during oxidative recycling of sulphide (Canfield & Teske 1996; Detmers *et al.* 2001). Sulphate and pyrite $\delta^{34}S$ trends broadly mirror one another, but pyrite is generally much more variable, attributable to the fact that reduction, oxidation and disproportionation reactions commonly occur during early diagenesis, where distinct local effects, such as pore water sulphate concentrations, availability of appropriate substrates for BSR, and physiology of the BSR population (Detmers *et al.* 2001) strongly influence the final sulphur-isotope signature.

Sulphur isotopes have been widely applied to problems in Precambrian Earth history. For example, a gradual increase in the spread of $\delta^{34}S_{pyrite}$ in shales ($\delta^{34}S_{sulphate}-\delta^{34}S_{pyrite}$ isotopic discrimination) broadly coincides with separate geological and geochemical evidence for a Neoproterozoic rise in the oxygenation of the Earth's environment (Canfield & Teske 1996; Fike *et al.* 2006). Originally, this isotopic shift was linked to the evolutionary radiation of sulphide-oxidizing bacteria (Canfield & Teske 1996), but recent evidence puts this evolutionary event much earlier (Johnston *et al.* 2005). Instead, this isotopic shift could have been caused by a rise in the importance of sulphide oxidation and disproportionation reactions during early diagenesis, which may be indirectly linked to oxygenation through seafloor redox changes. The $\delta^{34}S$ pyrite compilation is also the basis for the model that the global deep ocean became dominantly euxinic, rather than oxygenated, as massive banded iron-formation deposition came to a close in the late Palaeoproterozoic (Poulton *et al.* 2004). The Neoproterozoic is characterized by extraordinary fluctuations in both $\delta^{34}S_{pyrite}$ and $\delta^{34}S_{sulphate}$ in the Neoproterozoic, which are closely coupled to glacial events (Halverson & Hurtgen 2007). However, the extent to which these variations truly reflect global seawater sulphate compositions and environmental conditions is poorly established.

Highly precise measurement of all four sulphur isotopes (^{32}S, ^{33}S, ^{34}S, ^{36}S) has shown resolvable and consistent variations in the parameters $\Delta^{33}S$ and $\Delta^{36}S$, which can reflect both mass-independent (MIF) and mass-dependent fractionation (MDF) processes. MIF of sulphur isotopes has been applied to reconstructing

the evolution of atmospheric oxygen levels (Farquhar *et al.* 2000), but has not been systematically applied to the Neoproterozoic, when atmospheric O_2 concentrations likely exceeded the low level ($<10^{-5}$ present levels) required to suppress MIF fractionation in the atmosphere (Pavlov & Kasting 2002). On the other hand, variations in $\Delta^{33}S$ and $\Delta^{36}S$ resulting from MDF record information about specific sulphur transformations and pathways that cannot be gleaned from traditional measurements of $^{2}S/^{4}S$ alone (Johnston *et al.* 2005; Ono *et al.* 2006). Although not reviewed here, the technique of measuring quadruple sulphur isotopes promises to yield significant insight into behaviour of the sulphur cycle leading up to and following the Neoproterozoic glaciations.

Iron speciation

The impressive range of $\delta^{34}S_{pyrite}$ and $\delta^{34}S_{sulphate}$ values that are typical of the Neoproterozoic are commonly interpreted in terms of a low sulphate ocean (Halverson & Hurtgen 2007). This interpretation is consistent with the observation that seawater during the Neoproterozoic was occasionally rich in dissolved ferrous iron, based on the occurrence of iron formation. Iron-speciation studies shed further light on the redox state of the oceans and are being carried out increasingly on Neoproterozoic successions (Canfield *et al.* 2008). Redox conditions in the water column affect the speciation of iron in marine sediments. The highly reactive iron pool (Fe_{HR}) is that which is geochemically available during diagenesis and includes iron bound in carbonates, iron oxides and oxyhydroxides, and iron sulphides (Canfield 1989). Sediments deposited under an oxic water column tend to contain less reactive iron as a fraction of total sedimentary iron (Fe_{HR}/Fe_T) than those deposited under an anoxic water column, with a proposed cut-off at 0.38 (Raiswell *et al.* 1988; Lyons & Severmann 2006). Canfield *et al.* (2008) further proposed that the measure of pyrite-bound iron v. total reactive iron (Fe_{Py}/Fe_{HR}) can be used to distinguish iron-rich anoxic v. euxinic water columns, with sediments exhibiting $Fe_{Py}/Fe_{HR} > 0.8$ being classified as euxinic.

Neoproterozoic sediments deposited beneath a storm wave base typically exhibit high Fe_{HR}/Fe_T ratios (Fig. 4.1), indicating that anoxia was common in the deeper marine environment. However, sulphidic conditions are so far only indicated during the pre-glacial Neoproterozoic and early Cambrian (Canfield *et al.* 2008), suggesting ferruginous rather than sulphidic (euxinic) anoxia during the interval of climatic fluctuations. Because ferruginous conditions can only arise when the molar flux of Fe_{HR} to the deep ocean is greater than half the flux of sulphide, their reappearance during the Neoproterozoic after an absence of more than a billion years is consistent with a low-sulphate ocean reservoir.

Strontium isotopes

Over timescales of $>10^6$ years, the $^{87}Sr/^{86}Sr$ ratio of seawater records the relative strontium fluxes from continental weathering and hydrothermal input, superimposed on the long-term increase in $^{87}Sr/^{86}Sr$ as a result of radioactive decay of ^{87}Rb (Edmond 1992). As such, marine $^{87}Sr/^{86}Sr$ is a useful measure of evolving tectonic and long-term climatic regimes. Nevertheless, the ensemble of driving mechanisms for the variations in seawater $^{87}Sr/^{86}Sr$ spanning the Neoproterozoic remains controversial. It is doubtful that seawater $^{87}Sr/^{86}Sr$ can be simplified to a simple balance between the hydrothermal and continental inputs, but rather must also be influenced by continental configuration and CO_2 outgassing rates (Halverson *et al.* 2007; Shields 2007).

Strontium-isotope stratigraphy is based on the presumption that seawater was always isotopically homogeneous with respect to Sr because of its long ocean residence time. Although isotopic analysis is now standard procedure, samples need to be carefully screened because of the risk of contaminating the sample with diagenetically altered or detrital materials. This risk is reduced for Phanerozoic studies for which microscopically well-preserved low-Mg calcite tests (e.g. foraminifera, brachiopods and belemnites) can be analysed. However, for much of the Precambrian, it is necessary to identify least altered components of the bulk carbonate rock (e.g. Derry *et al.* 1992; Kaufman *et al.* 1993).

Strontium isotope analysis comprises the following six steps, of which the first four vary considerably between research groups: (i) sample selection using petrographic and geochemical criteria; (ii) physical extraction from the host sample; (iii) chemical pre-treatment to remove contaminant Sr ions; (iv) sample dissolution; (v) chemical separation of the element Sr; (vi) mass spectrometric analysis. Studies show that least altered ratios can most easily be obtained by targeted microsampling of fine-grained calcite (micrite), which is free of later recrystallization and dolomitization, although early diagenetic cements may also be reliable tracers of ocean composition (e.g. Kaufman *et al.* 1993; Fairchild *et al.* 2000). Chemical pre-leaching helps remove contaminant Rb and radiogenic Sr (Gorokhov *et al.* 1995), while subsequent incomplete dissolution in weak acids such as acetic acid has been shown to limit inadvertent dissolution of clay mineral-bound Sr (Bailey *et al.* 2000).

The Neoproterozoic strontium-isotope record is typically reconstructed from calcite that has relatively high strontium and low rubidium concentrations or otherwise exhibits evidence of limited exchange with diagenetic fluids, as measured, for example, in Mn/Sr ratios (Brand & Veizer 1981; Jacobsen & Kaufman 1999). Although carbonate originally precipitated as aragonite is intrinsically more suitable due to its high original Sr content (Kulp *et al.* 1952), the abundance of metastable carbonate precipitates in the Precambrian indicates that some apparently pristine components could be the result of diagenetic replacement (Fairchild *et al.* 2000). Because alteration usually increases the $^{87}Sr/^{86}Sr$ of carbonates (Banner & Hanson 1990), the lowest measured values within a suite of rocks are typically inferred to most closely approximate the composition of the seawater from which it precipitated. However, this ought not merely to be assumed, as post-depositional fluids are not always more radiogenic than coeval seawater. With this in mind, least-altered ratios are best extrapolated from diagenetic trends, for example by plotting Mn/Sr, Mg/Ca, 1/Sr or $\delta^{18}O$ against measured $^{87}Sr/^{86}Sr$.

Recent compilations of the $^{87}Sr/^{86}Sr$ evolution of Neoproterozoic oceans share the common, dominant feature of ratios rising from as low as *c*. 0.7055 in the early Neoproterozoic to as high as 0.7085 in the Ediacaran Period (Jacobsen & Kaufman 1999; Walter *et al.* 2000; Melezhik *et al.* 2001; Halverson *et al.* 2007*a*; Shields 2007). This feature alone makes strontium-isotope chemostratigraphy a key tool in establishing correlations and relative age in otherwise poorly radiometrically dated Neoproterozoic successions. Additional detail in the strontium-isotope record remains controversial due to the relatively poor resolution of the Neoproterozoic record and variable quality of samples used in compilations (Melezhik *et al.* 2001). However, an apparently reproducible finer-scale structure in the record is emerging with the promise of improving the Neoproterozoic chronology and the link between coupled tectonic–climatic processes. Importantly, and as will be discussed further below, the seawater strontium-isotope record appears to be distinct, spanning each of the Neoproterozoic glacial epochs (Table 4.1).

The pre-glacial Neoproterozoic

The most characteristic features of the Neoproterozoic chemostratigraphic record are the generally high $\delta^{13}C_{carb}$ values that prevail throughout most of the era and the episodic negative anomalies

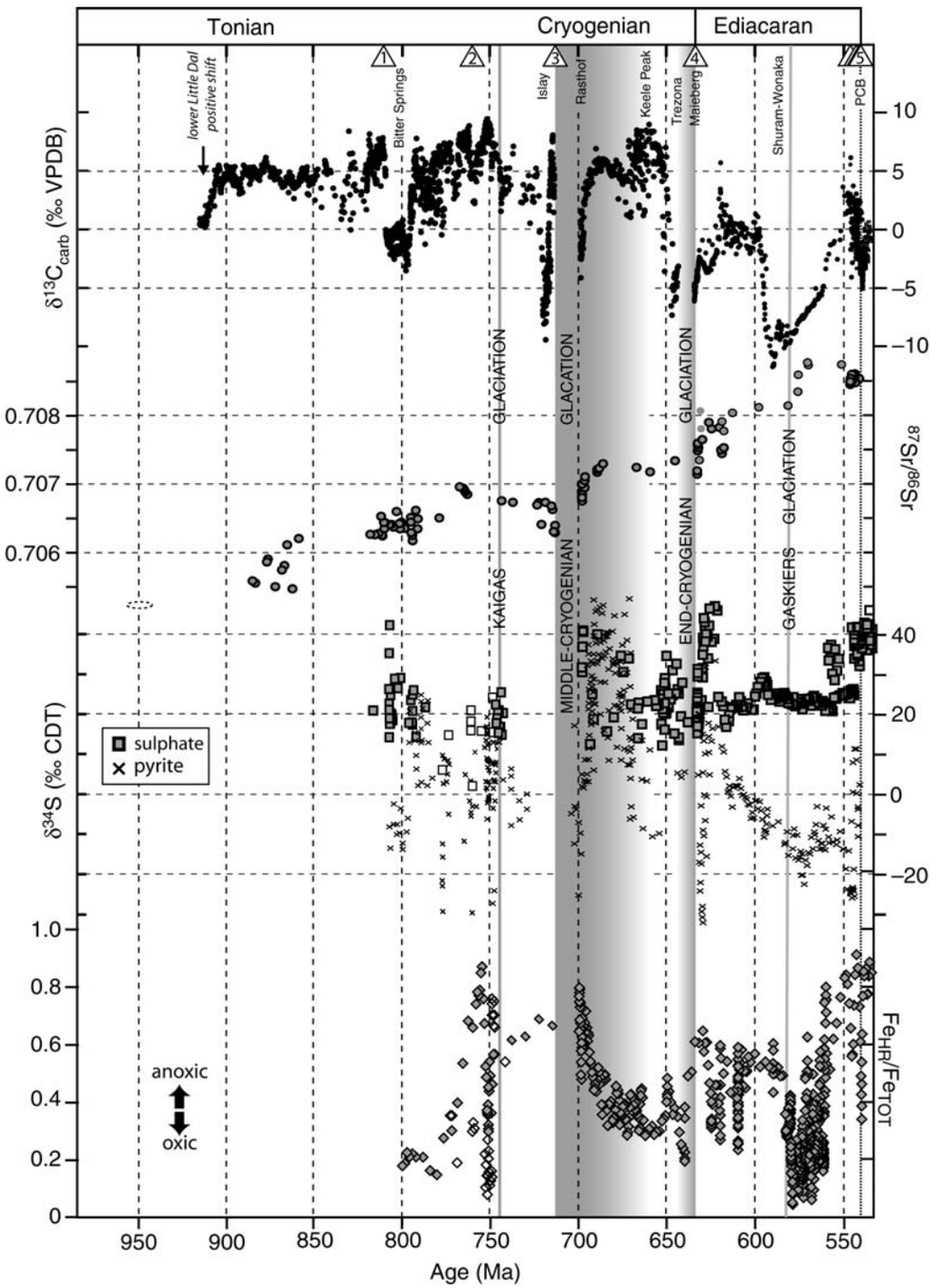

Fig. 4.1. Working chemostratigraphic compilations of $\delta^{13}C_{carb}$, $^{87}Sr/^{86}Sr$, $\delta^{34}S_{sulphate}$, $\delta^{34}S_{pyrite}$ and iron-speciation (Fe_{HR}/Fe_T) data for the Neoproterozoic (modified after Halverson *et al.* 2005, 2007*a*, 2010; Halverson 2006; Canfield *et al.* 2008). This compilation does not include all available high-quality data due to the difficulty of integrating data that have poor and variable age constraints (see text for discussion). The names shown vertically in the top of the figure are the informal names of the principal negative anomalies, as well as the distinct positive shift in $\delta^{13}C_{carb}$ recorded in the lower Little Dal Group (Halverson 2006) and the 'Keele Peak' positive anomaly (Kaufman *et al.* 2007). Note that there are conflicting sulphur-isotope data, in particular for the late Ediacaran Period (e.g. Ries *et al.* 2009). A low of $^{87}Sr/^{86}Sr$ in the earliest Neoproterozoic (dashed oval) is based on data from Gorokhov *et al.* (1995). Iron-speciation data (Fe_{HR}/Fe_T) are from Canfield *et al.* (2008), replotted as five-point running averages, and from Nagy *et al.* (2009). Open boxes and diamonds are additional $\delta^{34}S_{sulphate}$ and iron-speciation data from the Chuar Group as published in Johnston *et al.* (2010). Principle U–Pb geochronological constraints on the $\delta^{13}C_{carb}$ record are shown in triangles at the top of the compilation: (1) an 811.5 $\pm$ 0.3 Ma tuff in the Fifteenmile Group, Yukon Territory (Macdonald *et al.* 2010*b*); (2) a 760 $\pm$ 1 Ma tuff in the Ombombo Subgroup, NW Namibia (Halverson *et al.* 2005); (3) a 716.5 $\pm$ 0.2 Ma tuff in the lower Rapitan Group, Yukon Territory (Macdonald *et al.* 2010*b*); (4) an ash bed in the Ghaub Formation in northern Namibia dated at 635 $\pm$ 0.6 Ma (Hofmann *et al.* 2005) and an ash bed in the lower Duoshantuo Formation in South China dated at 635.2 $\pm$ 0.6 Ma (Condon *et al.* 2005) bracket the age of the Cryogenian–Ediacaran boundary; (5) a 542.0 $\pm$ 0.6 Ma ash bed at the Precambrian–Cambrian boundary in Oman (Amthor *et al.* 2003); and several slightly older ages (overlapping triangles) from the latest Ediacaran of the Nama Group, S Namibia (Grotzinger *et al.* 1995). Shaded boxes and lines show the inferred range of glacial events, with the gradational shading in the middle Cryogenian box reflecting the wide range of ages for middle Cryogenian glaciation (e.g. Allen & Etienne 2008).

that punctuate it (Knoll *et al.* 1986; Kaufman & Knoll 1995; Shields & Veizer 2002). These basic observations raise several questions. First, when did the average values near 0‰ typical of the Mesoproterozoic (Brasier & Lindsay 1995) give way to the average values of +5‰ (Halverson *et al.* 2005) characteristic of the Neoproterozoic? Second, did the increased variability in $\delta^{13}C_{carb}$ accompany the higher average values and, if not, when did this begin? Finally, what drove these fundamental shifts in the behaviour of the exogenic carbon cycle?

These questions are difficult to answer because of the poor carbon-isotope coverage and radiometric ages spanning the Mesoproterozoic–Neoproterozoic transition. Bartley *et al.* (2001) and Frank *et al.* (2003) argued that the increase in the amplitude and frequency of fluctuations in $\delta^{13}C_{carb}$ began sometime in the middle to late Mesoproterozoic, based on data from Siberia and NE Canada, respectively. Halverson (2006) argued that sustained $\delta^{13}C_{carb} \geq 5‰$ did not start until the early Neoproterozoic based on data from the Platform Assemblage of the Little Dal Group in NW Canada, where the lowermost data show a distinct ramp from 0 to 5‰ (Fig. 4.1), followed by generally high (≥5‰) values up to the onset of the Bitter Springs anomaly (see below). However, the age and correlation of the lowermost Little Dal Group and its equivalence to other rocks within Succession B in NW Canada is not known and only constrained to be between *c.* 1004 (Rainbird *et al.* 1996) and 811 Ma (Macdonald *et al.* 2010*b*). It is therefore unclear whether the lower Little Dal positive $\delta^{13}C$ shift (Fig. 4.1) truly does record the first highly ^{13}C-enriched seawater in the Neoproterozoic, or what the precise age of this event might be.

Much better constrained now is the timing of presumably the first major negative $\delta^{13}C_{carb}$ excursion in the Neoproterozoic: the *Bitter Springs anomaly* (Table 4.1; Halverson *et al.* 2005). Although older negative $\delta^{13}C_{carb}$ excursions have been reported (Bartley *et al.* 2001; Shields 2007), these are generally from poorly dated successions and may be the result of alteration. For example, ^{13}C-depleted I6 unit rocks of the Atar Group, Mauritania (Shields 2007), although now known to be *c.* 1.1 Ga in age (Rooney *et al.* 2010), are likely to have undergone significant isotopic alteration (Fairchild *et al.* 1990). The *Bitter Springs* negative anomaly was first fully documented in the Bitter Springs Formation in the Amadeus basin of central Australia (Hill *et al.* 2000). It was subsequently recorded in more detail in Svalbard (Halverson *et al.* 2005), where it is clearly defined by reciprocal $\delta^{13}C$ shifts of >8‰ that perfectly coincide with rare exposure surfaces in the Akademikerbreen Group. The anomaly also appears to occur in the upper Little Dal Group (Upper Carbonate Formation) in the Mackenzie Mountains (Halverson 2006). These global correlations are reinforced by additional geochemical data (Halverson *et al.* 2007*a*), namely $^{87}Sr/^{86}Sr$ (see below) and an updated and high-resolution $\delta^{13}C_{carb}$ record through the Bitter Springs Formation (Swanson-Hysell *et al.* 2010), as well as the coincidence of the shifts with prominent sequence boundaries. Both features have been interpreted to relate to large true polar wander episodes (Maloof *et al.* 2006).

The *Bitter Springs anomaly* (Table 4.1; Fig. 4.1) has now been reproduced across northwestern Canada: within the middle Lower Tindir Group (Tatunduk Inlier), upper Fifteenmile Group (Coal Creek Inlier), and the Wynniatt Formation of the Shaler Supergroup (Victoria Island; Macdonald *et al.* 2010*b*; Jones *et al.* 2010), although in this latter case only the negative shift is preserved and this is recorded in sediments intruded by mafic sills, which means it may be an overprint related to contact metamorphism rather than a primary signal. A likely correlative has also been documented in the Tambien Group of northern Ethiopia (Alene *et al.* 2006; Miller *et al.* 2009). Macdonald *et al.* (2010*b*) produced a precise U–Pb zircon age of 811.51 ± 0.25 Ma on a tuff *c.* 50 m beneath the negative shift presumed to define the base of the anomaly in upper Fifteenmile Group, thus constraining the onset of the Bitter Springs anomaly to *c.* 810 Ma and providing a more robust basis for global correlations. At the upper boundary of the Bitter Springs anomaly, $\delta^{13}C_{carb}$ shifts back to values exceeding 5‰.

The $\delta^{13}C_{carb}$ of seawater at the time of the putative and possibly regional Kaigas (Bayisi) glaciation at *c.* 750–740 Ma (Frimmel *et al.* 1996; Xu *et al.* 2009) is not well known. Negative $\delta^{13}C$ values occur in the lower Wallekraal Formation, which overlies the Kaigas Formation (Fölling & Frimmel 2002) but no large $\delta^{13}C$ anomaly occurs between the Bitter Springs anomaly and the Islay anomaly in Svalbard (Fig. 4.1). Instead, $\delta^{13}C_{carb}$ values remain generally high until the onset of the Islay anomaly (Prave *et al.* 2009), which appears to precede the first major Cryogenian glaciation (Fig. 4.1) and is discussed in more detail in the following section.

The strontium-isotope record through the early Neoproterozoic shown in Figure 4.1 is largely derived from data from Svalbard and northwestern Canada, even though other presumably primary values have been obtained from other successions such as the Bitter Springs Formation. As noted by Bartley *et al.* (2001), seawater $^{87}Sr/^{86}Sr$ values reach a nadir around the Mesoproterozoic–Neoproterozoic transition, presumably related to the final assembly of Rodinia. The least radiogenic latest Mesoproterozoic $^{87}Sr/^{86}Sr$ values reported by Bartley *et al.* (2001) hover around 0.7055, which is virtually the same as a value of 0.7056 from limestones of the Atar Group, Taoudeni Basin (Veizer *et al.* 1983), now dated at 1.1 Ga (Rooney *et al.* 2010) and the lowest values in the lower Little Dal Group (Halverson *et al.* 2007*a*). However, Gorokhov *et al.* (1995) reported values from pristine limestones of the presumed early Neoproterozoic Burovaya Formation (Turukhansk uplift, NW Siberia) as low as 0.7052. Thus, 0.7055 is a plausible approximation for seawater $^{87}Sr/^{86}Sr$ at the Mesoproterozoic–Neoproterozoic boundary, but probably does not represent the nadir before the protracted Neoproterozoic rise in $^{87}Sr/^{86}Sr$.

Strontium-isotope ratios had risen to 0.7063 by the onset of the Bitter Springs anomaly (Fig. 4.1). Although a more discreet and smaller shift to slightly higher ratios accompanies the negative $\delta^{13}C$ shift at the base of the anomaly, $^{87}Sr/^{86}Sr$ returns to *c.* 0.7063 at the end of the Bitter Springs anomaly, before apparently increasing to as high as 0.7070 in the Backlundtoppen Formation in Svalbard (prior to the Islay anomaly). No intervening data from this transition have been documented. As will be discussed below, this middle Neoproterozoic $^{87}Sr/^{86}Sr$ peak is followed by a temporary return to values as low as 0.7063.

The sulphur-isotope record for the early Neoproterozoic is relatively sparse, despite the fact that voluminous evaporites were deposited in Australia and NW Canada *c.* 830 to 800 Ma (Evans 2006). Indeed, the compilation in Figure 4.1 does not include any data older than *c.* 820 Ma, although this lacuna is in part an artefact of poor control on ages and correlations, which limit the data that can be used. $\delta^{34}S_{sulphate}$ from evaporites in the Gillen Member of the Bitter Springs Formation (i.e. before the Bitter Springs anomaly) ranges from 15 to 21‰ (Gorjan *et al.* 2000; Hill *et al.* 2000). From the available data, it appears that early Neoproterozoic seawater $\delta^{34}S_{sulphate}$ values do not depart greatly from the Gillen Member values (Fig. 4.1), averaging *c.* 20‰ through the middle Neoproterozoic, close to average values for the Cretaceous and Cenozoic (Paytan *et al.* 1998, 2004; Kampschulte & Strauss 2004), but distinct from the highly ^{34}S-enriched values that characterize the early and late Ediacaran and early Palaeozoic (Shields *et al.* 2004; Kampschulte & Strauss 2004; Halverson & Hurtgen 2007).

Although most $\delta^{34}S_{sulphate}$ data of the composite curve for this time interval are derived from CAS measurements on Svalbard samples (Halverson *et al.* 2010), available data from evaporites spanning the Bitter Springs anomaly in the Amadeus Basin (Gorjan *et al.* 2000; Hill *et al.* 2000) yield similar values. Pyrite data in this record are also sparse and similarly derived mainly from Svalbard (Halverson *et al.* 2010) and the Bitter Springs

Table 4.1. *Summary of the $\delta^{13}C_{carb}$ and $^{87}Sr/^{86}Sr$ signatures associated with the major Neoproterozoic negative carbon isotope anomalies (Fig. 4.1) and an abridged compilation of locations where they are well preserved (for the Maieberg and Rasthof anomalies, only key locations where the anomalies are preserved in great detail are given). PB, Paraguai Belt; UTG, Upper Tindir Group*

Shuram-Wonoka anomaly

$\delta^{13}C_{carb}$	Minimum: $< -10‰$; protracted recovery
$^{87}Sr/^{86}Sr$	0.7081–0.7084

Region	Unit	Reference
S Namibia	Nama Gp	Workman *et al.* (2002)
Oman	Shuram/Kufai Fm	Burns & Matter (1993), Le Guerroué *et al.* (2006)
S China	Doushantuo Fm	Jiang *et al.* (2007), McFadden *et al.* (2008)
S Australia	Wonoka Fm	Pell *et al.* (1993), Calver (2000)
N Norway	Nyborg Fm	Halverson *et al.* (2005)
SW USA	Johnnie Fm	Corsetti & Kaufman (2003)
SE Siberia	Nikol'skaya/Chenchinskaya	Pokrovskii *et al.* (2006), Melezhik *et al.* (2009)

Maieberg anomaly

$\delta^{13}C_{carb}$	Minimum: −4 to −6‰, gradual to abrupt return to near 0‰ values
$^{87}Sr/^{86}Sr$	0.7072 at base, increases upsection to 0.7078–0.7080

Region	Unit	Reference
NW Namibia	Maieberg Fm	Hoffman *et al.* (1998)
S Namibia	Bloeddrif Mb	Fölling & Frimmel (2002)
Oman	Hadash/Masirah Bay	Le Guerroué *et al.* (2006)
NW China	Tureeken Fm	Xiao *et al.* (2004)
S China	Doushantuo Fm	Jiang *et al.* (2007), McFadden *et al.* (2008) and others
SW Mongolia	Oi Mb	Macdonald *et al.* (2009*a*)
E Svalbard	Dracoisen Fm	Kaufman *et al.* (1997), Halverson *et al.* (2004)
Scotland	Cranford Ls	McCay *et al.* (2006)
NE Alaska	Katakturuk Dolomite (K2)	Macdonald *et al.* (2009*b*)
SW USA	Noonday Dolomite	Prave (1999)
Brazil (PB)	Araras Fm	Nogueira *et al.* (2007)
SE Siberia	Barakunskaya Fm	Pokrovskii *et al.* (2006), Melezhik *et al.* (2009)

Trezona anomaly

$\delta^{13}C_{carb}$	Minimum: −6 to −8‰, increases before glaciation
$^{87}Sr/^{86}Sr$	0.7072–0.7074

Region	Unit	Reference
NW Namibia	Ombaatjie Fm	Halverson *et al.* (2002)
South Australia	Trezona Fm	McKirdy *et al.* (2001)
N Norway	Grasdal Fm	Halverson *et al.* (2005)
Scotland	Craignish/Ardrishaig	Prave *et al.* (2009)
NE Alaska	Katakturuk Dolomite (K1)	Macdonald *et al.* (2009*b*)
Mackenzie Mts	Keele Fm	Halverson *et al.* (2005)

Rasthof anomaly

$\delta^{13}C_{carb}$	Minimum: −4 to 0‰, rises rapidly
$^{87}Sr/^{86}Sr$	0.7067–0.7069 at base, increases up section to 0.7072–0.7073

Region	Unit	Reference
NW Namibia	Rashtof Fm	Hoffman *et al.* (1998), Yoshioka *et al.* (2003)
SW Mongolia	Base Tayshir Mb	Shields *et al.* (1997), Macdonald *et al.* (2009*a*)
S Australia	Tapley Hill Fm	McKirdy *et al.* (2001)
Scotland	Bonahaven Fm*	Brasier & Shields (2000), McCay *et al.* (2006), Prave *et al.* (2009)
NE Alaska	Katakturuk Dolomite (K1)	Macdonald *et al.* (2009*b*)
Mackenzie Mts	Twitya Fm.	Hoffman & Schrag (2002)
SW USA	base Beck Spring Fm	Corsetti & Kaufman (2003)

Islay anomaly

$\delta^{13}C_{carb}$	Minimum: −5 to −9‰, return to >0‰ before glaciation
$^{87}Sr/^{86}Sr$	0.7065–0.7067, declines upsection to 0.7064

Region	Unit	Reference
Tasmania	Black River Fm	Calver (1998)
E Svalbard	Elbobreen Fm	Halverson *et al.* (2004)

(*Continued*)

Table 4.1. *Continued*

Scotland	Islay/Lossit Fm	Brasier & Shields (2000), Prave *et al.* (2009), McCay *et al.* (2006), Sawaki *et al.* (2010*b*)
E Greenland	Bed Group 19	Fairchild *et al.* (2000)
Victoria Island	Killian Formation	Macdonald *et al.* (2010*b*)
Mackenzie Mts	Copper Cap Fm	Halverson (2006)
Alaska-Yukon	Upper Dolomite (LTG)	Macdonald *et al.* (2010*a*)
SW USA	Upper Beck Spring Fm	Corsetti & Kaufman (2003)
Bitter Springs anomaly		
$\delta^{13}C_{carb}$	Minimum: −5 to 0‰, bracketed by sharp positive and negative shift	
$^{87}Sr/^{86}Sr$	0.7063–0.7065	
Region	**Unit**	**Reference**
N Ethiopia	Tambien Group	Alene *et al.* (2006)
Central Australia	Bitter Springs Formation	Hill *et al.* (2000)
Western Australia	Hussar Formation	Hill (2005)
E Svalbard	Grusdievbreen/Svanbergfjellet	Halverson *et al.* (2005)
Scotland	Ballachulish Sbgp	Prave *et al.* (2009)
Mackenzie Mts	Upper Carbonate Fm	Halverson (2006)
Yukon	Upper Fifteenmile Gp (PF1)	Macdonald *et al.* (2010*b*)
Alaska-Yukon	Upper Shale (LTG)	Macdonald *et al.* (2010*a*)

*Prave *et al.* (2009) argued that the post-Port Askaig negative $\delta^{13}C$ anomaly is missing, in which case the Bonahaven anomaly, which is stratigraphically above the glacigenic Port Askaig Formation, might be equivalent to the Tayshir anomaly in Mongolia.

Formation (Hill *et al.* 2000). The most salient pattern in the $\delta^{34}S$ data is a coupled increase in $\delta^{34}S_{sulphate}$ and decrease in $\delta^{34}S_{pyrite}$ coincident with the Bitter Springs anomaly (Fig. 4.1), resulting in a transient increase in $\Delta^{34}S$. Other constraints on the $\delta^{34}S_{sulphate}$ of early Neoproterozoic seawater come from studies on successions from Arctic Canada. $\delta^{34}S_{sulphate}$ values there range from 14 to 18‰ in the pre-Bitter Springs anomaly (>810 Ma) Gypsum Formation of the Little Dal Group (Turner 2009), while similar values (16–19‰) have been reported from the post-Bitter Springs anomaly (<780 Ma) Redstone River Formation of the overlying Coates Lake Group (Strauss 1993).

The sulphur-isotope record throughout the remainder of the early–middle Neoproterozoic is thin, but suggests a return to reduced $\Delta^{34}S$ resulting from higher average $\delta^{34}S_{pyrite}$ sometime prior to the middle Cryogenian glaciation.

Spanning the Cryogenian glaciations

Significant discussion remains as to the number, timing and duration of the Cryogenian glaciations, and the base of the Cryogenian period has yet to be formally defined. Two particular persistent sources of controversy and confusion are the possible occurrence of an early (*c.* 745–750 Ma; Borg *et al.* 2003) 'Kaigas' glaciation (Frimmel *et al.* 1996) that may not have been global in extent and the seemingly contradictory age constraints on the so-called 'Sturtian' or early Cryogenian glaciation. There is no incontrovertible evidence that the Kaigas diamictite in the Gariep belt of southern Namibia (see Macdonald *et al.* (2011) for a stratigraphic and sedimentological reappraisal of the Kaigas diamictites) and other older diamictites in the Katanga Supergroup in Zambia (Key *et al.* 2001) and NW China (Xu *et al.* 2009) are glacial in origin (Hoffman & Li 2009). Chemostratigraphic data spanning these isolated diamictites are also sparse. Therefore, although the putative Kaigas glaciation is plotted in Figure 4.1, we do not review the chemostratigraphic framework for this possible middle-Neoproterozoic glaciation. As for the sticky question of the age of early Cryogenian glaciation (i.e. glaciation between the older Kaigas event and the end-Cryogenian 'Marinoan' event), reviewed recently by Hoffman & Li (2009), we acknowledge that it is impossible to discriminate at this point between the model that there were multiple middle Cryogenian glaciations or a single, long-lived glacial epoch that spanned from *c.* 716 (Macdonald *et al.* 2010*b*) to 660 Ma (Fanning & Link 2008).

These deficiencies in the Cryogenian chronology are exacerbated by presumably larges hiatuses in the records on continental shelves (from whence most of the chemostratigraphic records are derived) resulting from glacioeustatic fall in sea level and glacial erosion. These complications in the Cryogenian record make it impossible to produce an accurate chemostratigraphic record for the Cryogenian period and the compilation in Figure 4.1 can only be regarded as a work in progress. Nevertheless, it is notable that independent compilations emerging from widely separate sedimentary basins do seem to be converging on a similar overall chemostratigraphic structure for the interval spanning the Cryogenian glaciations (e.g. Halverson *et al.* 2005; Prave *et al.* 2009; Macdonald *et al.* 2010*b*).

The negative $\delta^{13}C_{carb}$ anomalies that coincide with deglaciation and are preserved in transgressive–regressive sequences overlying glacial deposits and their equivalent glacial unconformities (i.e. cap carbonate sequences; Hoffman & Schrag 2002) are well documented (Table 4.1; Williams 1979; Kaufman *et al.* 1997; Kennedy *et al.* 1998; Halverson *et al.* 2005; Hoffman *et al.* 2007). Therefore, only the most important features are summarized here. Importantly, no more than two distinct, post-glacial negative $\delta^{13}C_{carb}$ anomalies linked to Cryogenian glaciation are known to occur in a single succession (Kennedy *et al.* 1998). Where there are two such post-glacial anomalies within one succession or, where there is just one of known age, consistent distinctions can be drawn between the two anomalies (Table 4.1; Kennedy *et al.* 1998; Hoffman & Schrag 2002).

As a general rule, the older of the two post-glacial sequences lacks the basal transgressive portion, meaning the maximum flooding surface is the base of the sequence (Hoffman & Schrag 2002; Hoffman *et al.* 2011). $\delta^{13}C_{carb}$ typically begins negative and trends positive, returning to values >0‰ within a few metres (Kennedy *et al.* 1998; Halverson *et al.* 2005). For example, in the Rasthof Formation of NW Namibia, $\delta^{13}C_{carb}$ begins at around −4.3‰ (herein referred to as the *Rasthof* anomaly) and crosses over abruptly to positive values *c.* 10 m up-section, at the contact

between a basal rhythmite member and an overlying chaotic microbialite member (Hoffman *et al.* 1998; Yoshioka *et al.* 2003). The thickness of this anomaly in Namibia is in large part a function of the amount of allodapic dolomite within the lower member (Halverson *et al.* 2005). Only in rare instances is a negative trend preserved in the lowermost part of the sequence (e.g. in the presumed Rasthof-equivalent basal Tayshir Member of the Tsagaan Oloom Formation, Mongolia; Macdonald *et al.* 2009*a*).

In contrast, the basal transgressive portion of the sequence overlying the end-Cryogenian glacials and defining the base of the Ediacaran Period (Knoll *et al.* 2006) commonly preserves an upward negative trend, with values typically in the range of −2 to −4‰ (Hoffman & Schrag 2002; Hoffman *et al.* 2007; Rose & Maloof 2010). In the carbonate-dominated post-glacial platformal sequence in NW Namibia (Maieberg Formation) where the *Maieberg* anomaly has been most extensively studied, $\delta^{13}C_{carb}$ continues to decline to nearly −6‰ at the maximum flooding surface before gradually returning to higher values over hundreds of metres of the section (Hoffman *et al.* 1998). However, this apparent protracted recovery is not typical of the basal Ediacaran negative $\delta^{13}C_{carb}$ anomaly, and in many other carbonate-dominated locations, including the slope equivalents of the Maieberg Formation in Namibia (Halverson *et al.* 2005), the Doushantuo Formation of South China (e.g. McFadden *et al.* 2008), and the Barakunskaya Formation in southern Siberia (Pokrovskii *et al.* 2006), the anomaly is relatively condensed, spanning only several metres to a few tens of metres. Thus, relative sedimentation rates must be considered when correlating chemostratigraphic signals.

Large negative $\delta^{13}C_{carb}$ anomalies also precede two Cryogenian glaciations (Table 4.1; Fig. 4.2). The so-called *Trezona* anomaly, named after the Trezona Formation in South Australia where the anomaly was first fully documented (McKirdy *et al.* 2001), occurs prior to the end-Cryogenian (i.e. the 'Marinoan' or 'Elatina' glaciation in South Australia) glaciation and following the so-called *Keele Peak* (Kaufman *et al.* 1997), where $\delta^{13}C_{carb}$ reaches values $\geq$+9‰ (Figs 4.1 & 4.2). This negative anomaly is best documented in the Ombaatjie Formation in the Otavi Group, NW Namibia, where it is defined by a gradual, facies-independent decline from *c.* +7 to −5‰ through up to 50 m of dominantly shallow-water carbonates, followed by a positive shift of a few ‰ (Halverson *et al.* 2002). The extent of truncation of the anomaly can be used as a general indicator of the depth of erosion on the glacial surface.

A negative anomaly of similar magnitude, referred to as the *Islay* anomaly (Prave *et al.* 2009) after the formation in Scotland (Figs 4.1 & 4.2) where it was first documented (Brasier & Shields 2000; McCay *et al.* 2006; Sawaki *et al.* 2010*a*), occurs prior to the older Cryogenian glaciation in several successions. In NE Svalbard, this anomaly is virtually identical in shape, magnitude and stratigraphic context to the Trezona anomaly in Namibia (Fig. 4.2) and is similarly variably erosionally truncated (Halverson *et al.* 2004). However, in Scotland, $\delta^{13}C$ returns to positive values prior to glaciation (Prave *et al.* 2009). In NW Canada and East Greenland, the presumably (but not definitively) equivalent anomalies in the Coates Lake Group (Halverson 2006) and Bed Groups 19–20 (Fairchild *et al.* 2000), respectively, feature an even more prominent positive shift, possibly providing an important distinction from the Trezona anomaly.

A potentially different late Cryogenian negative $\delta^{13}C_{carb}$ anomaly of similar magnitude has been found in the Tayshir Member of the lower Tsagaan Oloom Formation in Mongolia (Macdonald *et al.* 2009*a*). This anomaly has been tentatively correlated with the Bonahaven anomaly in Scotland (Prave *et al.* 2009) and an anomaly of much smaller magnitude in the Gruis Formation of NW Namibia, between the Rasthof and Trezona anomalies (Fig. 4.2). A similar large negative anomaly in this stratigraphic position has not been documented elsewhere. Therefore, it remains plausible that the anomaly in the Tayshir Member is equivalent to the Trezona anomaly and the return to positive $\delta^{13}C_{carb}$ values above the anomaly has been removed by erosion as it was in Namibia (Macdonald *et al.* 2009*a*).

Although the homologous pattern of the Islay and Trezona anomalies suggests a similar origin, it diminishes the utility of these anomalies for correlation purposes. Fortunately, the anomalies are clearly distinguished from one another chemostratigraphically by their strontium-isotope signatures. Whereas $^{87}Sr/^{86}Sr$ ratios of 0.7072–0.7073 coincide with the Trezona anomaly (Halverson *et al.* 2007*a*), $^{87}Sr/^{86}Sr$ through the older Islay anomaly distinctly declines from *c.* 0.7068 to 0.7064 (Fig. 4.2; Table 4.1), with the lowest values in the Islay Formation corresponding to the return towards positive $\delta^{13}C_{carb}$ values (Sawaki *et al.* 2010*a*). Similar $^{87}Sr/^{86}Sr$ values have been reported from the likely equivalent interval in the Coates Lake Group (0.7066; Halverson *et al.* 2007*a*) and Bed Group 20 (0.7063; Fairchild *et al.* 2000). Thus, it appears that the onset of the middle-Cryogenian glaciation is preceded by a 0.0005 decline in the $^{87}Sr/^{86}Sr$ of seawater following the *c.* 765 Ma peak of *c.* 0.7070 (Fig. 4.1) documented in the Backlundtoppen Formation. In contrast to this negative slope leading up to the middle Cryogenian glaciation, the $^{87}Sr/^{86}Sr$ record in the following interglacial interval has a positive slope (Fig. 4.1), with a smooth and seemingly rapid increase in $^{87}Sr/^{86}Sr$ from 0.7067 to 0.7073 recorded in the Tsagaan Oloom Formation in Mongolia (Shields *et al.* 1997).

Strontium-rich aragonite and barite cements of the Hayhook Formation in the upper part of the transgressive portion of the post-Ice Brook (base Ediacaran) sequence in the Mackenzie Mountains, NW Canada, have $^{87}Sr/^{86}Sr$ ratios of *c.* 0.70715 (Halverson *et al.* 2007*a*; Hoffman & Halverson 2011). These values are effectively indistinguishable from a ratio of 0.70718 measured within the pre-glacial Keele Peak in the same section (Halverson *et al.* 2007*a*) and therefore indicate no net change in $^{87}Sr/^{87}Sr$ spanning the end-Cryogenian glaciation.

The sulphur-isotope record spanning the Cryogenian glaciations is almost entirely based on pyrite and CAS (there being few evaporites during this time span) and is intensely variable (Fig. 4.1). This variability reflects a combination of low seawater sulphate concentrations and strongly fluctuating environmental conditions tied to global glaciation (Hurtgen *et al.* 2002), as well as possible post-depositional effects. Sulphur-isotope data (Fig. 4.1) from the Chuar Group in southwestern USA show a return to $\delta^{34}S_{pyrite}$ values clustering around 0‰ and low $\delta^{34}S$ values around 750 Ma, coinciding with at least local development of euxinic deep waters as determined from iron-speciation data on mid-shelf black shales (Johnston *et al.* 2010). Sulphur-isotope data are sparse for the subsequent interval leading up to the middle Cryogenian glaciation (i.e. the *c.* 717 Ma Rapitan glaciation; Macdonald *et al.* 2010*b*). However, abundant pyrite and CAS data have been produced from the interglacial interval, in particular from Namibia (Hurtgen *et al.* 2002; Gorjan *et al.* 2003) and Australia (Gorjan *et al.* 2000; McKirdy *et al.* 2001). Whereas $\delta^{34}S_{pyrite}$ data from within the Sturt and equivalent glacial units in Australia range from 0 to −20‰, they are strongly positive, with values commonly 20–60‰ in post-glacial rocks, such as the Tapley Hill, Aralka, Datangpo, Rasthof and lower Court formations (Fig. 4.1). This extreme, immediately post-glacial trend in pyrite values is matched by highly ^{34}S-enriched $\delta^{34}S_{sulphate}$ values from CAS, such that $\Delta^{34}S \approx 0$‰. $\delta^{34}S_{pyrite}$ values then decline precipitously in the middle interglacial period, paralleling a smaller decline in $\delta^{34}S_{sulphate}$, resulting in $\Delta^{34}S$ values approaching 30‰. $\Delta^{34}S$ reduces again just before the onset of the end-Cryogenian glaciation, coinciding with the Trezona negative $\delta^{13}C$ anomaly (Fig. 4.1; Table 4.1).

$\delta^{34}S$ values are again erratic immediately following the end-Cryogenian glaciation: a trend of rapidly increasing $\delta^{34}S_{sulphate}$ that coincides with a wide range in $\delta^{34}S_{pyrite}$ (−30 to +20‰) may be sufficient to distinguish this post-glacial (i.e.

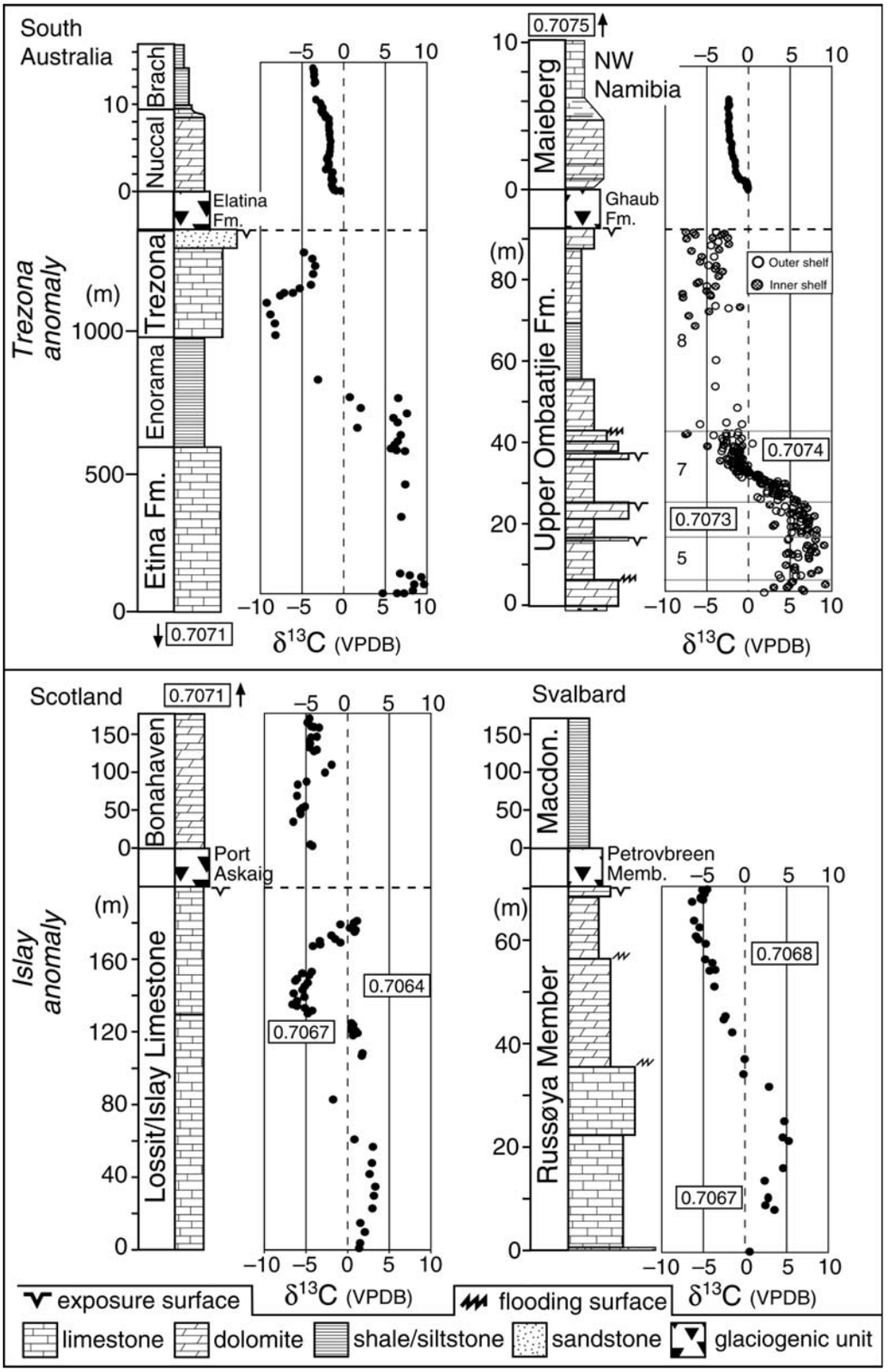

Fig. 4.2. Summary stratigraphic plots and accompanying $\delta^{13}C_{carb}$ profiles and $^{87}Sr/^{86}Sr$ data for key sections spanning the *Trezona* and *Islay* pre-glacial (Cryogenian) negative $\delta^{13}C$ anomalies. Note the variable scales across the non-scaled glaciogenic intervals in each column. Nucc, Nuccaleena Formation; Brach, Brachina Formation; Macdon., Macdonaldryggen Member. Australia data from McKirdy *et al.* (2001); Namibia data from Halverson *et al.* (2002, 2007*a*), which includes data from both the inner and outer continental shelf of the Ombaatjie Formation; Scotland data from Brasier & Shields (2000), McCay *et al.* (2006) and Prave *et al.* (2009); Svalbard data from Halverson *et al.* (2004, 2007*a*).

basal Ediacaran) sulphur-isotope record from the middle Cryogenian post-glacial record. However, coeval $\delta^{34}S$ profiles that vary from more proximal to more open ocean post-glacial sections in Namibia (Hurtgen *et al.* 2006) and South China (Li *et al.* 2010) suggest significant heterogeneity in the concentration and sulphur-isotope composition of seawater sulphate and generally low sulphate concentrations in the earliest Ediacaran Period. Therefore, sulphur-isotope chemostratigraphy may be useful in establishing an early Ediacaran age, but would not be reliable for detailed correlations for sedimentary rocks of this age.

The Ediacaran Period

The beginning of the Ediacaran Period coincides with a major negative $\delta^{13}C_{carb}$ anomaly (the *Maieberg* anomaly; Fig. 4.1) that punctuates the final global glaciation of the Neoproterozoic (Knoll *et al.* 2006), as discussed above. Although $\delta^{13}C_{carb}$ values return to near 0‰ within about 3 million years of the end of glaciation (Condon *et al.* 2005), they then remain relatively low for much of the early Ediacaran Period, with the exception of a positive spike to +6–10‰ seen in some sections, such as NW Namibia and NE

Svalbard (Halverson *et al.* 2005). This pattern contrasts with the sustained high $\delta^{13}C_{carb}$ values typical of much of the earlier Neoproterozoic.

Superimposed on the lower average $\delta^{13}C_{carb}$ values in the Ediacaran Period, the dominant feature in the record is the so-called *Shuram* (or *Shuram-Wonoka*) anomaly, named after the Shuram Formation in the Huqf Supergroup of Oman (Burns & Matter 1993). The Shuram anomaly features a precipitous drop to $\delta^{13}C_{carb}$ values $< -10‰$, followed by a protracted recovery back to values near 0‰ (Fig. 4.1). This extraordinary anomaly has been the subject of considerable recent research and controversy. However, despite arguments against a primary origin for the anomaly (Bristow & Kennedy 2008; Knauth & Kennedy 2009; Derry 2010), anomalies of strikingly similar magnitude, structure and approximate age occur in multiple sedimentary basins from across the globe (Table 4.1), including Sr-rich limestones in south-central Siberia (Pokrovskii *et al.* 2006; Melezhik *et al.* 2009). Thus, the most parsimonious interpretation is that the Shuram anomaly reflects a primary oceanographic phenomenon.

Despite the large number of chemostratigraphic data that have been obtained globally from rocks preserving the Shuram anomaly, the timing and duration of the anomaly and, indeed, the number of large Ediacaran negative $\delta^{13}C_{carb}$ anomalies remain controversial. For example, whereas $\delta^{13}C_{carb}$ records from thick, seemingly continuous carbonate-rich sections in Oman (Fike *et al.* 2006; Le Guerroué *et al.* 2006) and south-central Siberia (Pokrovskii *et al.* 2006) clearly show a single, long-lived negative $\delta^{13}C_{carb}$ anomaly, certain sections from the Doushantuo Formation, South China, show a pair of large-magnitude anomalies separated by $\delta^{13}C_{carb}$ values as high as +6‰ (Jiang *et al.* 2007; McFadden *et al.* 2008). Because the Doushantuo pattern is preserved in highly condensed sections (relative to sections from other successions) from a basin that was not demonstrably fully open to the global ocean and has not been reproduced globally, the more consistent and higher-resolution patterns derived from Oman and Siberia are favoured in the compilation in Figure 4.1. However, we acknowledge that the inconsistent patterns between the Doushantuo Formation and correlative units worldwide pose a problem for carbon-isotope chemostratigraphy.

Separate data sets from the Wonoka Formation, South Australia (Calver 2000), Oman (Fike *et al.* 2006) and South China (McFadden *et al.* 2008) also show a decoupling between the $\delta^{13}C_{carb}$ record spanning the Shuram anomaly and coeval organic carbon ($\delta^{13}C_{org}$) data (Calver 2000; Fike *et al.* 2006; McFadden *et al.* 2008), a pattern that lends support to the popular hypothesis that the Ediacaran ocean contained a large, reactive organic carbon pool that strongly modulated $\delta^{13}C_{carb}$ and the oxidation of the deep oceans (Rothman *et al.* 2003; Condon *et al.* 2005). However, the relationship between $\delta^{13}C_{carb}$ and $\delta^{13}C_{org}$ is not the same in these three successions. For example, $\delta^{13}C_{org}$ values are much more negative in South China than in Oman or South Australia, and $\delta^{13}C_{org}$ values are more variable through the main part of the anomaly in Oman than elsewhere. Therefore, the significance and reliability of the middle Ediacaran $\delta^{13}C_{org}$ record is unclear.

Of critical importance in reconstructing the connections between perturbations to the exogenic carbon cycle, global climate and biospheric evolution in the Ediacaran Period is the connection, if any, between the Shuram anomaly and the short-lived *c.* 580 Ma Gaskiers glaciation (Bowring *et al.* 2003). Is the Gaskiers glaciation, like the global Cryogenian glaciations, preceded by a large negative $\delta^{13}C$ anomaly? Unfortunately, no unambiguous evidence for both the glaciation and the full anomaly occurs in any single stratigraphic succession. Although Halverson *et al.* (2005) interpreted major erosional unconformities in successions hosting the Shuram anomaly, such as the Wonoka Formation (South Australia) and the Johnnie Formation (Death Valley), to be related to Gaskiers glacioeustasy, this argument remains speculative. The problem of resolving the relative timing between $\delta^{13}C$ anomalies and glaciation is exacerbated by the possibility that whereas the anomaly should be globally synchronous, the glaciation may be diachronous, or there may be multiple discrete glaciations (e.g. Chumakov 2010). Indeed, $\delta^{13}C_{carb}$ values are highly variable in relation to other reported Ediacaran glacial deposits, such as in the Kimberley of northern Australia, where positive $\delta^{13}C$ values characterize carbonates overlying the Egan Formation (Corkeron 2007, 2011). Other contrasting $\delta^{13}C_{carb}$ values are found in the Hankalchough Formation in the Tarim Basin, NW China (Xiao *et al.* 2004), and the Hongtiegou Formation in the Chaidam Basin, NW China (Shen *et al.* 2010). Some authors have even argued that some of the purported Ediacaran glacial deposits, such as the Hankalchough (Chumakov 2010) and the Hongtiegou (Shen *et al.* 2010) formations significantly post-date the Gaskiers glaciation (Chumakov 2009). Germs *et al.* (2009) argue for a latest Ediacaran (*c.* 547 Ma) 'Schwarzrand' glaciation based on evidence from the upper Nama Group, Namibia.

Notwithstanding the ambiguity in the age, timing, number and distribution of Ediacaran-aged glacial deposits, carbon-isotope data from the basal Ediacaran Nyborg Formation and the overlying glaciogenic Mortensnes Formation of the Varanger Peninsula, northern Norway, do appear to resolve the relative timing between at least one middle Ediacaran glaciation and the Shuram $\delta^{13}C_{carb}$ anomaly. Dolomite beds within Member E in the uppermost Nyborg Formation, in the least-truncated section beneath the major erosional unconformity at the base of the glaciogenic Mortensnes Formation (Edwards 1984), have $\delta^{13}C_{carb}$ compositions of −7.6 to −9.9‰, while the matrix of a carbonate-dominated diamictite within the Mortensnes Formation has a $\delta^{13}C_{carb}$ composition of −10.4‰ (see Rice *et al.* 2011). Because the Shuram anomaly is the only interval in the Ediacaran Period where $\delta^{13}C_{carb}$ values are known to drop below −7‰, these data are interpreted to indicate that the Mortensnes glaciation post-dated the nadir of the negative anomaly (Halverson *et al.* 2005). In this regard, an Ediacaran glaciation, although seemingly not global, may have been triggered by a similar mechanism as the Cryogenian glaciations.

The return to positive $\delta^{13}C_{carb}$ values following the Shuram anomaly occurs late in the Ediacaran, by *c.* 551 Ma, implying that the Ediacaran fauna first appeared during the anomaly (Condon *et al.* 2005). A subsequent, short-lived negative $\delta^{13}C$ anomaly coincides with the Precambrian–Cambrian boundary (Magaritz *et al.* 1986; Knoll *et al.* 1995; Saylor *et al.* 1998; Amthor *et al.* 2003), but there is no evidence to link this anomaly with a glaciation.

Strontium-isotope ratios from the Mackenzie Mountains indicate little net change in seawater $^{87}Sr/^{86}Sr$ spanning the end-Cryogenian glaciation (Fig. 4.2). However, data from strontium-rich limestones in the lower Maieberg Formation, NW Namibia, show a rapid rise in $^{87}Sr/^{86}Sr$ to values >0.7078 following post-glacial maximum flooding and prior to recovery in $\delta^{13}C_{carb}$ values to near 0‰ (Halverson *et al.* 2007; cf. Shields 2007). This positive spike in $^{87}Sr/^{86}Sr$ is a predictable result of extremely high CO_2 levels and corresponding elevated silicate weathering rates following deglaciation (Higgins & Schrag 2003). Simple geochemical modelling also implies that the spike to more radiogenic values should be short-lived, with $^{87}Sr/^{86}Sr$ approaching background values after CO_2 declined to more typical levels within a few million years of deglaciation (Le Hir *et al.* 2009). This decline may be recorded in data from the Una Group (Irecê basin) on the São Francisco Craton, Brazil (Misi & Veizer 1998), where the strontium- and carbonate-isotope compositions suggest an early Ediacaran age, consistent with recent detrital zircon data from the equivalent Bambui Group (Sial *et al.* 2010).

A much better established pattern in the Ediacaran strontium-isotope record is the subsequent rise to $^{87}Sr/^{86}Sr \geq 0.7080$ that characterizes the latter part of the Ediacaran Period (e.g. Kaufman *et al.* 1997; Jacobsen & Kaufman 1999; Shields 2007; Melezhik *et al.* 2009). Sawaki *et al.* (2010*b*) suggested additional

structure in the late Ediacaran record based on data they obtained from a drill core through the Doushantuo Formation, including a drop to <0.7080 prior to the Shuram anomaly and a peak in $^{87}Sr/^{86}Sr$ of 0.7090 coinciding with the protracted low $\delta^{13}C_{carb}$ of the anomaly. Regarding the high values, as for Oman, where similarly high values have been reported for the late Ediacaran (Burns *et al.* 1994), none of these highly enriched values is preserved in samples retaining high strontium concentrations. Conversely, strontium-rich limestones in the upper Doushantuo Formation in the core have $^{87}Sr/^{86}Sr$ values of *c.* 0.7085, similar to strontium-isotope data straddling the Precambrian–Cambrian boundary in other well-studied successions (Brasier *et al.* 1996; Kaufman *et al.* 1997; Saylor *et al.* 1998). Gaucher *et al.* (2009) report $^{87}Sr/^{86}Sr$ values of <0.7080 in the late Ediacaran Arroyo del Soldado Group on the Rio de la Plata craton, lending support to the possibility that $^{87}Sr/^{86}Sr$ may have indeed fluctuated strongly in the late Ediacaran Period, much as it did in the subsequent Early Cambrian (Halverson *et al.* 2010). Evidently, much work remains in elucidating the fine structure in the late Ediacaran $^{87}Sr/^{86}Sr$ record.

The relationship between middle Ediacaran $^{87}Sr/^{86}Sr$ and the Gaskiers (or other Ediacaran) glaciation is virtually unconstrained. However, strontium-isotope data from highly strontium-enriched limestones in southern Siberia show $^{87}Sr/^{86}Sr = 0.7081$ at about the level of the nadir in the Shuram anomaly, followed by an increase towards 0.7086 up-section, but still within the range of very low $\delta^{13}C_{carb}$ (Pokrovskii *et al.* 2006; Melezhik *et al.* 2009).

Anomalously ^{34}S-enriched seawater sulphate compositions bookend the Ediacaran Period (Fig. 4.1) in many successions. As discussed above, variable, but predominantly high $\delta^{34}S_{suphate}$ and low $\Delta^{34}S$ values near 0‰ prevail in the basal Ediacaran Period (Fig. 4.1). By the early Cambrian, $\delta^{34}S_{sulphate}$, as measured in a variety of minerals, including evaporites, francolite and carbonate, was again high (35–40‰) in most basins (e.g. Holser & Kaplan 1966; Strauss 1993; Shields *et al.* 1999; Kampschulte & Strauss 2004). However, $\delta^{34}S_{sulphate}$ from the late Ediacaran in South China (McFadden *et al.* 2008) and southern Namibia (Ries *et al.* 2009) are generally lower, with concomitant decreases in $\Delta^{34}S$. The source of this substantial spatial variability in the late Ediacaran sulphur-isotope record, whether oceanographic, related to post-depositional influences or analytical artefacts, is not resolved.

The Ediacaran sulphur-isotope record as compiled in Figure 4.1 comprises a detailed data set of $\delta^{34}S_{sulphate}$ (CAS) and $\delta^{34}S_{pyrite}$ data from the Nafun Group, Oman (Fike *et al.* 2006) and pyrite data from the Pertatataka Formation, central Australia (Gorjan *et al.* 2000). The Oman record, together with other fragmentary data (Fig. 4.1), indicates that more typical $\delta^{34}S_{sulphate}$ values close to 20‰ are the norm for the Ediacaran Period, although evaporite and CAS data appear to be contradictory at times (cf. Fike *et al.* 2006 with Schröder *et al.* 2004). At the same time, data from both Oman and central Australia display a spike to positive $\delta^{34}S_{pyrite}$ values in the early Ediacaran Period, followed by a gradual decrease through the middle Ediacaran Period, resulting in a steady increase in $\delta^{34}S$, a predictable result of increasing seawater sulphate concentrations (Halverson & Hurtgen 2007).

Average $\delta^{34}S_{pyrite}$ values in the deepwater Conception Group (Avalon Peninsula, SE Newfoundland; Canfield *et al.* 2007) show a decrease from about +20 to 0‰ across the Gaskiers glaciation, but the $\delta^{34}S_{sulphate}$ record spanning the glaciation is unknown. Iron-speciation data indicate ferruginous (and presumably low sulphate) conditions during the Gaskiers glaciation (Canfield *et al.* 2008). Detailed $\delta^{34}S_{sulphate}$ (CAS) records have been produced across the onset of the Shuram–Wonoka anomaly. In Oman, a spike in $\delta^{34}S_{sulphate}$ to +29‰ coincides with the anomaly (Fike *et al.* 2006). Across the presumably equivalent interval in Death Valley (Kaufman *et al.* 2007) and South China (McFadden *et al.* 2008), $\delta^{34}S_{sulphate}$ decreases to values <20‰. Thus, although $\delta^{34}S$ records show tantalizing connections with other major Ediacaran events, either $\delta^{34}S$ compositions of late Neoproterozoic seawater sulphate were highly heterogeneous (Ries *et al.* 2009), inferred correlations are inaccurate, or the measured sulphur-isotope compositions in some or all of the sedimentary successions do not preserve reliable signatures of primary seawater composition.

Discussion and conclusions

Precise radiometric ages are the gold standard for drawing precise interbasinal correlations, particularly in the absence of a robust biostratigraphy. Direct ages are also required for calibrating the sedimentary record, but they are frustratingly rare in most of the successions that archive important information about the evolution of Earth's surface environment in the Neoproterozoic. Thus, other tools and many assumptions are required to merge the fragmentary records from across the globe into one coherent Neoproterozoic chronology. Isotope chemostratigraphy has long been heralded as a possible solution (Knoll & Walter 1992). Insofar as the popular proxies for ocean chemistry ($\delta^{13}C$, $\delta^{34}S$, $^{87}Sr/^{86}Sr$) are reliable, geologists can characterize the Neoproterozoic record one fragment at a time. Accordingly, isotope geochemistry has been widely applied to stratigraphic studies of the Neoproterozoic, with a strong focus on the glaciogenic record.

An intimate relationship between extreme perturbations to the global carbon cycle, as recorded in the marine $\delta^{13}C_{carb}$ record, and episodes of widespread glaciation (Knoll *et al.* 1986) has long been the starting point for these studies. However, even as this fundamental observation about the behaviour of the Neoproterozoic Earth has withstood the test of time, diverse studies from across the world have added important new details to this broad pattern. Long-lived positive carbon-isotope trends had been ascribed to pre-glacial oceanographic conditions, while negative carbon-isotope anomalies were attributed to post-glacial 'cap carbonates', providing for elegantly simple models for the interrelation between $\delta^{13}C_{carb}$, carbon burial, atmospheric CO_2 and glaciation (e.g. Kaufman *et al.* 1997). The recognition that a large negative $\delta^{13}C_{carb}$ anomaly actually preceded the end-Cryogenian glaciation shattered this model of a simple cause-and-effect relationship between the two and opened the door for the compelling but controversial Snowball Earth hypothesis (Hoffman *et al.* 1998), which continues to dominate the debate about the Neoproterozoic glaciations.

It is now recognized that negative $\delta^{13}C$ anomalies also precede middle Cryogenian (McCay *et al.* 2006; Prave *et al.* 2009; Macdonald *et al.* 2010*b*) and middle Ediacaran glaciations (Halverson *et al.* 2005). Furthermore, in all cases, it appears that the initiation of glaciation followed a return towards positive $\delta^{13}C_{carb}$ values after the $\delta^{13}C_{carb}$ minima, thus further complicating an already complex relationship between the anomalies and global cooling. This motif in the coupled $\delta^{13}C$-climate record renders using the carbon-isotope record alone for global correlations insufficient, but fortunately it projects upon a marine strontium-isotope record with a strong unidirectional trend (Fig. 4.1). $^{87}Sr/^{86}Sr$ increases steadily during the Neoproterozoic from 0.7055 around the Mesoproterozoic–Neoproterozoic boundary to 0.7085 at the Neoproterozoic–Palaeozoic boundary, interrupted by only a few significant but short-lived declines (Fig. 4.1). Consequently, seawater $^{87}Sr/^{86}Sr$ ratios are different for each of the large negative anomalies associated with the Neoproterozoic glaciations (Table 4.1). The potential of strontium isotopes as a tracer of global environmental change remains to be fully realized. However, abrupt rises, most notably following the Cryogenian glaciations, are consistent with enhanced chemical weathering after glaciation. Conversely, changes in seawater $^{87}Sr/^{86}Sr$ appear to have been relatively muted during glaciations.

At this stage, the Neoproterozoic record is now sufficiently well understood that the combination of carbon- and strontium-isotope

stratigraphy, particularly if integrated with stratigraphic and sedimentological data, enables confident correlations and assignment of robust, if only relative, ages on carbonate-rich successions that otherwise lack firm age control. High-quality data sets spanning variable portions of the Neoproterozoic record and tied to an increasing number of precise U–Pb zircon ages have now been produced from across the world (e.g. Macdonald *et al.* 2010*b*). The result is a convergence in carbon- and strontium-isotope compilations towards a consistent pattern, even if many of the finer details remain obscure.

The integrated stratigraphic, $\delta^{13}C$ and $^{87}Sr/^{86}Sr$ records serve as a chronological template to the Neoproterozoic onto which other secular data sets can be added, such as sulphur-isotope compositions, redox specific data, biomarkers and biostratigraphy. The sulphur-isotope record is patchy, particularly for the first half of the Neoproterozoic, and highly variable, with clear instances where data sets spanning equivalent-aged rocks from different parts of the world, and even single basins, are not consistent with one another. Thus, much work remains to be done to establish the reliability of the sulphur-isotope proxy and the causes, either related to oceanographic conditions or diagenetic process, for the high degree of scatter in the record. Nevertheless, several of the salient patterns, mostly notably extremely high $\delta^{34}S_{sulphate}$ and $\delta^{34}S_{pyrite}$ values, are temporally linked to glaciation, indicating that the record can be used to help reconstruct the palaeoenvironmental evolution of Neoproterozoic ocean chemistry. Specifically, large variations in $\delta^{34}S$ of sulphate and pyrite and the difference between these two values in coeval sediments ($\Delta^{34}S$) is an indirect measure of fluctuations in the redox state of global seawater (Hurtgen *et al.* 2005). The sustained and very high $\delta^{34}S_{pyrite}$ (20–60‰) values recorded in the post-Sturtian Tapley Hill–Aralka formations in Australia (Gorjan *et al.* 2000) and the peak in $\delta^{34}S_{sulphate}$ straddling the Precambrian–Cambrian boundary stand out as unique chronostratigraphic markers in the otherwise noisy sulphur-isotope record (Fig. 4.1).

Iron-speciation data has become a popular new tool for reconstructing water column redox conditions (Lyons & Severmann 2006) that has been successfully applied to the Neoproterozoic (e.g. Canfield *et al.* 2007, 2008). Although it remains to be shown that distinct trends can be correlated beyond a single basin (Johnston *et al.* 2010), or are even consistent within a single basin, sharp fluctuations in normalizsed highly reactive iron content in shales (Fe_{HR}/Fe_T), for example, are closely linked to glaciation and other proxy evidence for oscillations in the redox chemistry of the oceans (Canfield *et al.* 2007, 2008). Although not discussed here, many other chemostratigraphic proxies show great promise for tracing evolving redox conditions through the Neoproterozoic and evaluating the highly unusual environment in the aftermath of global glaciations (Halverson *et al.* 2010, and references therein). Furthermore, biostratigraphy is increasingly being tightly integrated with chemostratigraphic data in order to evaluate more closely the connections between biospheric and biogeochemical change (e.g. McFadden *et al.* 2008; Nagy *et al.* 2009; Macdonald *et al.* 2010*a*). Thus, there is little doubt that chemostratigraphy will continue to elucidate the finer details in the number, timing and correlation of Neoproterozoic glaciations and the environmental conditions leading up to and following them.

This represents a contribution of the IUGS- and UNESCO-funded IGCP (International Geoscience Programme) Project #512.

References

Alene, M., Jenkin, G. R. T., Leng, M. J. & Darbyshire, D. P. F. 2006. The Tambien Group, Ethiopia: An early Cryogenian (ca. 800–735 Ma) Neoproterozoic sequence in the Arabian–Nubian Shield. *Precambrian Research*, **147**, 79–99.

Allen, P. A. & Etienne, J. L. 2008. Sedimentary challenge to Snowball Earth. *Nature Geoscience*, **1**, 817–825.

Amthor, J. E., Grotzinger, J. P., Schröder, S., Bowring, S. A., Ramezani, J., Martin, M. W. & Matter, A. 2003. Extinction of *Cloudina* and *Namacalathus* at the Precambrian–Cambrian boundary in Oman. *Geology*, **31**, 431–434.

Bahlburg, H. & Dobrzinski, N. 2011. A review of the Chemical Index of Alteration (CIA) and its application to the study of Neoproterozoic glacial deposits and climate transitions. *In*: Arnaud, E., Halverson, G. P. & Shields-Zhou, G. (eds) *The Geological Record of Neoproterozoic Glaciations*. Geological Society, London, Memoirs, **36**, 81–92.

Bailey, T. R., McArthur, J. M., Prince, H. & Thirlwall, M. F. 2000. Dissolution methods for strontium isotope stratigraphy: whole rock analysis. *Chemical Geology*, **167**, 313–319.

Banner, J. L. & Hanson, G. N. 1990. Calculation of simultaneous isotopic and trace element variations during water–rock interaction with applications to carbonate diagenesis. *Geochimica et Cosmochimica Acta*, **54**, 3123–3137.

Bao, H., Lyons, J. R. & Zhou, C. 2008. Triple oxygen isotope evidence for elevated CO_2 levels after a Neoproterozoic glaciation. *Nature*, **453**, 504–506.

Bartley, J. K., Semikhatov, M. A., Kaufman, A. J., Knoll, A. H., Pope, M. C. & Jacobsen, S. B. 2001. Global events across the Mesoproterozoic–Neoproterozoic boundary: C and Sr isotopic evidence from Siberia. *Precambrian Research*, **111**, 165–202.

Borg, G., Kärner, K., Buxton, M., Armstrong, R. & van der Merwe, S. W. 2003. Geology of the Skorpion supergene zinc deposit, southern Namibia. *Economic Geology*, **98**, 749–771.

Bowring, S., Myrow, P., Landing, E., Ramezani, J. & Grotzinger, J. 2003. Geochronological constraints on terminal Proterozoic events and the rise of the Metazoans. *Geophysical Research Abstracts (EGS, Nice)*, **50**, 13219.

Brand, U. & Veizer, J. 1981. Chemical diagenesis of a multicomponent carbonate system – 2: stable isotopes. *Journal of Sedimentary Petrology*, **51**, 987–997.

Brasier, M. D. & Lindsay, J. F. 1995. A billion years of environmental stability and the emergence of eukaryotes: New data from northern Australia. *Geology*, **26**, 555–558.

Brasier, M. D. & Shields, G. 2000. Neoproterozoic chemostratigraphy and correlation of the Port Askaig glaciation, Dalradian Supergroup of Scotland. *Journal of the Geological Society, London*, **157**, 909–914.

Brasier, M. D., Shields, G. A., Kuleshov, V. N. & Zhegallo, E. A. 1996. Integrated chemo- and biostratigraphic calibration of early animal evolution: Neoproterozoic–early Cambrian of southwest Mongolia. *Geological Magazine*, **133**, 445–485.

Bristow, T. F. & Kennedy, M. J. 2008. Carbon isotope excursions and the oxidant budget of the Ediacaran atmosphere and ocean. *Geology*, **36**, 863–866.

Burns, S. J. & Matter, A. 1993. Carbon isotopic record of the latest Proterozoic from Oman. *Eclogae Geologicae Helvetiae*, **86**, 595–607.

Burns, S. J., Haudenschild, U. & Matter, A. 1994. The strontium isotopic composition of carbonates from the late Precambrian (<560–540 Ma) Huqf Group of Oman. *Chemical Geology*, **111**, 269–282.

Calver, C. 2000. Isotope stratigraphy of the Ediacaran (Neoproterozoic III) of the Adelaide rift complex, Australia, and the overprint of water column stratification. *Precambrian Research*, **100**, 121–150.

Canfield, D. E. 1989. Reactive iron in marine sediments. *Geochimica et Cosmochimica Acta*, **53**, 619–632.

Canfield, D. E. & Teske, A. 1996. Late Proterozoic rise in atmospheric oxygen concentration inferred from phylogenetic and sulfur-isotope studies. *Nature*, **382**, 127–132.

Canfield, D. E., Poulton, S. W., Knoll, A. H., Narbonne, G. M., Ross, G., Goldberg, T. & Strauss, H. 2008. Ferruginous conditions dominated later Neoproterozoic deep-water chemistry. *Science*, **321**, 949–952.

Canfield, D. E., Poulton, S. W. & Narbonne, G. M. 2007. Late-Neoproterozoic deep-ocean oxygenation and the rise of animal life. *Science*, **315**, 92–95.

Chumakov, N. M. 2009. The Baykonurian Glaciohorizon of the Late Vendian. *Stratigraphy and Geological Correlation*, **17**, 373–381.

Chumakov, N. M. 2010. Neoproterozoic glacial events in Eurasia. *In*: Gaucher, C., Sial, A. N., Halverson, G. P. & Frimmel, H. E. (eds) *Neoproterozoic-Cambrian Tectonics, Global Change and Evolution: A Focus on Southwestern Gondwana*. Developments in Precambrian Geology, **16**. Elsevier, Dordrecht, 389–403.

Condon, D., Zhu, M., Bowring, S., Jin, Y., Wang, W. & Yang, A. 2005. From the Marinoan glaciation to the oldest bilaterians: U–Pb ages from the Doushantou Formation, China. *Science*, **308**, 95–98.

Corkeron, M. 2007. 'Cap carbonates' and Neoproterozoic glacigenic successions from the Kimberly region, north-west Australia. *Sedimentology*, **54**, 871–903.

Corkeron, M. 2011. Neoproterozoic glacial deposits of the Kimberly Region and northwestern Northern Territory, Australia. *In*: Arnaud, E., Halverson, G. P. & Shields-Zhou, G. (eds) *The Geological Record of Neoproterozoic Glaciations.* Geological Society, London, Memoirs, **36**, 659–672.

Corsetti, F. A. & Kaufman, A. J. 2003. Statigraphic investigations of carbon-isotope anomalies and Neoproterozoic ice ages in Death Valley, California. *Geological Society of America Bulletin*, **115**, 916–932.

Cozzi, A., Allen, P. A. & Grotzinger, J. P. 2004. Understanding carbonate ramp dynamics from C profiles: Examples from the Neoproterozoic Buah Formation of Oman. *Terra Nova*, **16**, 62–67.

Derry, L. A. 2010. A burial diagenesis origin for the Ediacaran Shuram-Wonoka anomaly. *Earth and Planetary Science Letters*, **295**, 152–162.

Derry, L. A., Kaufman, A. J. & Jacobsen, S. B. 1992. Sedimentary cycling and environmental change in the Late Proterozoic: evidence from stable and radiogenic isotopes. *Geochimica et Cosmochimica Acta*, **56**, 1317–1329.

Detmers, J., Brüchert, V., Habicht, K. S. & Kuever, J. 2001. Diversity of sulfur isotope fractionations by sulfate-reducing prokaryotes. *Applied and Environmental Microbiology*, **67**, 888–894.

Edmond, J. M. 1992. Himalayan tectonic, weathering processes, and strontium isotope record in marine limestones. *Science*, **258**, 1594–1597.

Edwards, M. B. 1984. Sedimentology of the Upper Proterozoic glacial record, Vestertana Group, Finnmark, North Norway. *Norges geologiske Undersøkelse Bulletin*, **394**, 1–76.

Evans, D. A. D. 2006. Proterozoic low orbital obliquity and axial-dipolar geomagnetic field from evaporite paleolatitudes. *Nature*, **444**, 51–55.

Fairchild, I. J., Marshall, J. D. & Bertrand-Sarfati, J. 1990. Stratigraphic shifts in carbon isotopes from Proterozoic stromatolitic carbonates (Mauritania): influences of primary mineralogy and diagenesis. *American Journal of Science*, **290A**, 46–79.

Fairchild, I. J., Spiro, B., Herrington, P. M. & Song, T. 2000. Controls on Sr and C isotope compositions of Neoproterozoic Sr-rich limestones of East Greenland and North China. *In*: Grotzinger, J. & James, N. (eds) *Carbonate Sedimentation, Diagenesis in an Evolving Precambrian World*. SEPM Special Publication, **67**, 297–313.

Fanning, C. M. & Link, P. K. 2008. *Age constraints for the Sturtian glaciation: data from the Adelaide Geosyncline, South Australia and Pocatello Formation, Idaho, USA*. Selwyn Symposium 2008, Geological Society of Australia, Extended Abstracts, **91**, 57–62.

Farquhar, J., Bao, H. & Thiemens, M. 2000. Atmospheric influence of Earth's earliest sulfur cycle. *Science*, **289**, 756–758.

Fike, D. A., Grotzinger, J. P., Pratt, L. M. & Summons, R. E. 2006. Oxidation of the Ediacaran ocean. *Nature*, **444**, 744–747.

Fölling, P. G. & Frimmel, H. W. 2002. Chemostratigraphic correlation of carbonate successions in the Gariep and Saldania belts, Namibia and South Africa. *Basin Research*, **14**, 69–88.

Frank, T. D., Kah, L. C. & Lyons, T. W. 2003. Changes in organic matter production and accumulation as a mechanism for isotopic variation in the Mesoproterozoic ocean. *Geological Magazine*, **140**, 397–420.

Frimmel, H. 2009. Trace element distribution in Neoproterozoic carbonates as palaeoenvironmental indicator. *Chemical Geology*, **258**, 338–353.

Frimmel, H. W., Klötzi, U. S. & Siegfried, P. R. 1996. New Pb/Pb single zircon age constraints on the timing of Neoproterozoic glaciation and continental break-up in Namibia. *The Journal of Geology*, **104**, 459–469.

Gaucher, C., Sial, A. N., Poiré, D., Gómez-Peral, L., Ferreira, V. P. & Pimentel, M. M. 2009. Chemostratigraphy. Neoproterozoic–Cambrian evolution of the Río de la Plata Palaeocontinent. *In*: Gaucher, C., Sial, A. N., Halverson, G. P. & Frimmel, H. E. (eds) *Neoproterozoic–Cambrian Tectonics, Global Change and Evolution: A Focus on Southwestern Gondwana*. Developments in Precambrian Geology, **16**, 115–122.

Germs, G. J. B., Miller, R. McG., Frimmel, H. E. & Gaucher, C. 2009. Syn- to late-orogenic sedimentary basins of southwestern Africa. Neoproterozoic to Early Palaeozoic evolution of Southwestern Africa. *In*: Gaucher, C., Sial, A. N., Halverson, G. P. & Frimmel, H. E. (eds) *Neoproterozoic–Cambrian Tectonics, Global Change and Evolution: A Focus on Southwestern Gondwana*. Developments in Precambrian Geology, **16**, 183–203.

Gorjan, P., Veevers, J. J. & Walter, M. R. 2000. Neoproterozoic sulfur-isotope variation in Australia and global implications. *Precambrian Research*, **100**, 151–179.

Gorjan, P., Walter, M. R. & Swart, R. 2003. Global Neoproterozoic (Sturtian) post-glacial sulfide-sulfur isotope anomaly recognised in Namibia. *Journal of African Earth Sciences*, **36**, 89–98.

Gorokhov, I. M., Semikhatov, M. A., Baskakov, A. V., Kutyavin, E. P., Melnikov, N. N., Sochava, A. V. & Turchenko, T. L. 1995. Sr isotopic composition in Riphean, Vendian, and Lower Cambrian carbonates from Siberia. *Stratigraphy and Geological Correlation*, **3**, 1–28.

Grotzinger, J. P., Bowring, S. A., Saylor, B. Z. & Kaufman, A. J. 1995. Biostratigraphic and geochronologic constraints on early animal evolution. *Science*, **270**, 598–604.

Halverson, G. P. 2006. A Neoproterozoic Chronology. *In*: Xiao, S. & Kaufman, A. J. (eds) *Neoproterozoic Geobiology and Paleobiology*. Springer, 231–271.

Halverson, G. P. & Hurtgen, M. T. 2007. Ediacaran growth of the marine sulfate reservoir. *Earth and Planetary Science Letters*, **263**, 32–44.

Halverson, G. P., Hoffman, P. F., Schrag, D. P. & Kaufman, A. J. 2002. A major perturbation of the carbon cycle before the Ghaub glaciation (Neoproterozoic) in Namibia: prelude to snowball Earth? *Geochemistry, Geophysics, Geosystems*, **3**, 10.1029/2001GC000244.

Halverson, G. P., Maloof, A. C. & Hoffman, P. F. 2004. The Marinoan glaciation (Neoproterozoic) in Svalbard. *Basin Research*, **16**, 297–324.

Halverson, G. P., Hoffman, P. F., Schrag, D. P., Maloof, A. C. & Rice, A. H. 2005. Towards a Neoproterozoic composite carbon-isotope record. *Geological Society of America Bulletin*, **117**, 1181–1207.

Halverson, G. P., Dudas, F. O., Maloof, A. C. & Bowring, S. A. 2007*a*. Evolution of the $^{87}Sr/^{86}Sr$ composition of Neoproterozoic seawater. *Palaeogeography, Palaeoclimatology, Palaeoecology*, **256**, 103–129.

Halverson, G. P., Maloof, A. C., Schrag, D. P., Dudas, F. O. & Hurtgen, M. T. 2007*b*. Stratigraphy and geochemistry of a ca 800 Ma negative carbon isotope interval in northeastern Svalbard. *Chemical Geology*, **237**, 5–27.

Halverson, G. P., Wade, B. P., Hurtgen, M. T. & Barovich, K. M. 2010. Neoproterozoic chemostratigraphy. *Precambrian Research*, **182**, 337–350.

Hayes, J. M., Kaplan, I. R. & Wedeking, K. W. 1983. Precambrian organic geochemistry, preservation of the record. *In*: Schopf, J. W. (ed.) *Earth's Earliest Biosphere. Its Origin and Evolution*. Princeton University Press, 93–134.

Hayes, J. M., Strauss, H. & Kaufman, A. J. 1999. The abundance of ^{13}C in marine organic matter and isotopic fractionation in the global biogeochemical cycle of carbon during the past 800 Ma. *Chemical Geology*, **161**, 103–125.

Higgins, J. A. & Schrag, A. P. 2003. Aftermath of a snowball Earth. *Geochemistry, Geophysics, Geosystems*, **4**, 1028.

Hill, A. C. 2005. Stable isotope stratigraphy, GSWA Lancer 1, Officer Basin, Western Australia. *In*: Mory, A. J. & Haines, P. W. (eds) *GSWA Lancer 1 Well Completion Report (Interpretive Papers)*

Officer and Gunbarrel Basins, Western Australia. Western Australia Geological Survey Record 2005/4, 1–11.

Hill, A. C., Arouri, K., Gorjan, P. & Walter, M. R. 2000. Geochemistry of marine and non-marine environments of a Neoproterozoic cratonic carbonate/evaporite: the Bitter Springs Formation, Central Australia. *In*: Grotzinger, J. P. & James, N. P. (eds) *Carbonate Sedimentation and Diagenesis in an Evolving Precambrian World*. SEPM Tulsa Special Publications, **67**, 327–344.

Hoffman, P. F. & Halverson, G. P. 2011. Neoproterozoic glacial record in the Mackenzie Mountains, northern Canadian Cordillera. *In*: Arnaud, E., Halverson, G. P. & Shields-Zhou, G. (eds) *The Geological Record of Neoproterozoic Glaciations*. Geological Society, London, Memoirs, **36**, 397–411.

Hoffman, P. F. & Li, Z.-X. 2009. A palaeogeographic context for Neoproterozoic glaciation. *Palaeogeography, Palaeoclimatology, Palaeoecology*, **277**, 158–172.

Hoffman, P. F. & Schrag, D. P. 2002. The snowball Earth hypothesis: testing the limits of global change. *Terra Nova*, **14**, 129–155.

Hoffman, P. F., Kaufman, A. J., Halverson, G. P. & Schrag, D. P. 1998. A Neoproterozoic snowball Earth. *Science*, **281**, 1342–1346.

Hoffman, P. F., Halverson, G. P., Domack, E. W., Husson, J. M., Higgins, J. A. & Schrag, D. P. 2007. Are basal Ediacaran (635 Ma) post-glacial 'cap dolostones' diachronous? *Earth and Planetary Science Letters*, **258**, 114–131.

Hoffman, P. F., Macdonald, F. A. & Halverson, G. P. 2011. Chemical sediments associated with Neoproterozoic glaciations: iron formation, cap carbonate, barite and phosphorite. *In*: Arnaud, E., Halverson, G. P. & Shields-Zhou, G. (eds) *The Geological Record of Neoproterozoic Glaciations.* Geological Society, London, Memoirs, **36**, 67–80.

Hoffmann, K. H., Condon, D. J., Bowring, S. A. & Crowley, J. L. 2004. A U–Pb zircon date from the Neoproterozoic Ghaub Formation, Namibia: constraints on Marinoan glaciation. *Geology*, **32**, 817–820.

Holser, W. T. 1997. Geochemical events documented in inorganic carbon isotopes. *Palaeogeography, Palaeoclimatology, Palaeoecology*, **132**, 173–182.

Holser, W. T. & Kaplan, I. R. 1966. Isotope geochemistry of sedimentary sulfates. *Chemical Geology*, **1**, 93–135.

Hough, M. L., Shields, G. A., Evins, L. Z., Strauss, H., Henderson, R. A. & Mackenzie, S. 2006. A major sulphur-isotope event at *c*. 510 Ma: a possible anoxia–extinction–volcanism connection during the Early–Middle Cambrian transition? *Terra Nova*, **18**, 257–263.

Hsu, K. J., Oberhänsli, H., Gao, J. Y., Shu, S., Haihong, C. & Krähenbühl, U. 1985. 'Strangelove ocean' before the Cambrian explosion. *Nature*, **316**, 809–811.

Hurtgen, M. T., Arthur, M. A., Suits, N. & Kaufman, A. J. 2002. The sulfur isotopic composition of Neoproterozoic seawater sulfate: implications for snowball Earth? *Earth and Planetary Science Letters*, **203**, 413–429.

Hurtgen, M. T., Halverson, G. P., Arthur, M. A. & Hoffman, P. F. 2006. Sulfur cycling in the aftermath of a Neoproterozoic (Marinoan) snowball glaciation: Evidence for a syn-glacial sulfidic deep ocean. *Earth and Planetary Science Letters*, **245**, 551–570.

Jacobsen, S. B. & Kaufman, A. J. 1999. The Sr, C, and O isotopic evolution of Neoproterozoic seawater. *Chemical Geology*, **161**, 37–57.

Jiang, G., Kaufman, A. J., Christie-Blick, N., Zhang, S. & Wu, H. 2007. Carbon isotope variability across the Ediacaran Yangtzee platform in South China: Implications for a large surface-to-deep ocean gradient. *Earth and Planetary Science Letters*, **261**, 303–320.

Johnston, D. T., Schmitz, M. D. *et al.* 2005. Active microbial sulfur disproportionation in the Mesoproterozoic. *Science*, **310**, 1477–1479.

Johnston, D. T., Poulton, S. W., Dehler, C., Porter, S., Husson, J., Canfield, D. E. & Knoll, A. H. 2010. An emerging picture of Neoproterozoic ocean chemistry: Insights from the Chuar Group, Grand Canyon, USA. *Earth and Planetary Science Letters*, **290**, 64–73.

Jones, D. S., Maloof, A. C., Hurtgen, M. T., Rainbird, R. H. & Schrag, D. P. 2010. Regional and global chemostratigraphic correlation of the early Neoproterozoic Shaler Sueprgroup, Victoria Island, Northwestern Canada. *Precambrian Research*, **181**, 43–63.

Kampschulte, A. & Strauss, H. 2004. The sulfur isotopic evolution of Phanerozoic seawater based on the analysis of structurally substituted sulfate in carbonates. *Chemical Geology*, **204**, 255–286.

Kasemann, S. A., Hawkesworth, C. J., Prave, A. R., Fallick, A. E. & Pearson, P. 2005. Boron and calcium isotope composition in Neoproterozoic carbonate rocks from Namibia: evidence for extreme environmental change. *Earth and Planetary Science Letters*, **231**, 73–86.

Kaufman, A. J. & Knoll, A. H. 1995. Neoproterozoic variations in the C-isotopic composition of seawater. *Precambrian Research*, **73**, 27–49.

Kaufman, A. J., Hayes, J. M., Knoll, A. H. & Germs, G. J. B. 1991. Isotopic composition of carbonates and organic carbon from upper Proterozoic successions in Nambia. *Precambrian Research*, **49**, 301–327.

Kaufman, A. J., Jacobsen, S. B. & Knoll, A. H. 1993. The Vendian record of Sr and C isotopic variations in seawater: Implications for tectonics and paleoclimate. *Earth and Planetary Science Letters*, **120**, 409–430.

Kaufman, A. J., Knoll, A. H. & Narbonne, G. M. 1997. Isotopes, ice ages, and terminal Proterozoic earth history. *Proceedings of the National Academy of Science (USA)*, **94**, 6600–6605.

Kaufman, A. J., Corsetti, F. A. & Varni, M. A. 2007. The effect of rising atmospheric oxygen on carbon and sulfur isotope anomalies in the Neoproterozoic Johnnie Formation, Death Valley, USA. *Chemical Geology*, **237**, 47–63.

Kennedy, M. J., Runnegar, B., Prave, A. R., Hoffmann, K.-H. & Arthur, M. 1998. Two or four Neoproterozoic glaciations? *Geology*, **26**, 1059–1063.

Kennedy, M. J., Christie-Blick, N. & Sohl, L. E. 2001. Are Proterozoic cap carbonates and isotopic excursions a record of gas hydrate destabilization following Earth's coldest intervals? *Geology*, **29**, 443–446.

Key, R. M., Liyungu, A. K., Njamu, F. M., Somwe, V., Banda, J., Mosley, P. N. & Armstrong, R. A. 2001. The western arm of the Lufilian Arc in NW Zambia and its potential for copper mineralization. *Journal of African Earth Sciences*, **33**, 503–528.

Knauth, L. P. & Kennedy, M. J. 2009. The late Precambrian greening of the Earth. *Nature*, **460**, 728–732.

Knoll, A. H. 2000. Learning to tell Neoproterozoic time. *Precambrian Research*, **100**, 3–20.

Knoll, A. H. & Walter, M. R. 1992. Latest Proterozoic stratigraphy and Earth history. *Nature*, **356**, 673–677.

Knoll, A. H., Hayes, J. M., Kaufman, A. J., Swett, K. & Lambert, I. B. 1986. Secular variation in carbon isotope ratios from Upper Proterozoic successions of Svalbard and east Greenland. *Nature*, **321**, 832–837.

Knoll, A. H., Grotzinger, J. P., Kaufman, A. J. & Kolosov, P. 1995. Integrated approaches to terminal Proterozoic stratigraphy: An example from the Olenek Uplift, northeastern Siberia. *Precambrian Research*, **73**, 251–270.

Knoll, A. H., Walter, M. R., Narbonne, G. M. & Christie-Blick, N. 2006. The Ediacaran Period: a new addition to the geologic time scale. *Lethaia*, **39**, 13–30.

Kulp, J. L., Turekian, K. & Boyd, D. W. 1952. Strontium content of limestones and fossils. *Geological Society of America Bulletin*, **63**, 701–716.

Le Guerroué, E., Allen, P. A., Cozzi, A., Etienne, J. L. & Fanning, M. 2006. 50 Myr recovery from the largest negative $\delta^{13}C$ excursion in the Ediacaran ocean. *Terra Nova*, **18**, 147–153.

Le Hir, G., Donnadieu, Y. *et al.* 2009. The snowball Earth aftermath: Exploring the limits of continental weathering processes. *Earth and Planetary Science Letters*, **277**, 453–463.

Li, C., Love, G. D., Lyons, T. W., Fike, D. A., Sessions, A. L. & Chu, X. 2010. A stratified redox model for the Ediacaran Ocean. *Science*, **328**, 80–83.

Lyons, T. W. & Severmann, S. 2006. A critical look at iron paleoredox proxies: New insights from modern euxinic marine environments. *Geochimica et Cosmochimica Acta*, **70**, 5698–5722.

Macdonald, F. A., Jones, D. S. & Schrag, D. P. 2009*a*. Stratigraphic and tectonic implications of a newly discovered glacial diamictite-cap carbonate couplet in southwestern Mongolia. *Geology*, **37**, 123–126.

MACDONALD, F. A., MCCLELLAND, W. C., SCHRAG, D. P. & MACDONALD, W. P. 2009*b*. Neoproterozoic glaciation on a carbonate platform margin in Arctic Alaska and the origin of the North Slope subterrane. *Geological Society of America Bulletin*, **121**, 448–473.

MACDONALD, F. A., COHEN, P. A., DUDÁS, F. O. & SCHRAG, D. P. 2010*a*. Early Neoproterozoic scale microfossils in the Lower Tindir Group of Alaska and the Yukon Territory. *Geology*, **38**, 143–146.

MACDONALD, F. A., SCHMITZ, M. D. *ET AL.* 2010*b*. Calibrating the Cryogenian. *Science*, **327**, 1241–1243.

MACDONALD, F. A., STRAUSS, J. V., ROSE, C., DUDÁS, F. Ö. & SCHRAG, D. P. 2011. Stratigraphy of the Port Nolloth Group of Namibia and South Africa, and implications for the age of Neoproterozoic iron formations. *American Journal of Science*, **310**, 862–888.

MAGARITZ, M., HOLSER, W. T. & KIRSCHVINK, J. L. 1986. Carbon-isotope events across the Precambrian/Cambrian boundary on the Siberian Platform. *Nature*, **320**, 258–259.

MALOOF, A. C., HALVERSON, G. P., KIRSCHVINK, J. L., SCHRAG, D. P., WEISS, B. P. & HOFFMAN, P. F. 2006. Combined paleomagnetic, isotopic, and stratigraphic evidence for true polar wander from the Neoproterozoic Akademikerbreen Group, Svalbard, Norway. *Geological Society of America Bulletin*, **118**, 1099–2014.

MARENCO, P. J., CORSETTI, F. A., KAUFMAN, A. J. & BOTTJER, D. J. 2008*a*. Environmental and diagenetic variations in carbonate associated sulfate: An investigation of CAS in the Lower Triassic of the western USA. *Geochimica et Cosmochimica Acta*, **72**, 1570–1582.

MARENCO, P. J., CORSETTI, F. A., HAMMOND, D. E., KAUFMAN, A. J. & BOTTJER, D. J. 2008*b*. Oxidation of pyrite during extraction of carbonate associated sulfate. *Chemical Geology*, **247**, 124–132.

MCCAY, G. A., PRAVE, A. R., ALSOP, G. I. & FALLICK, A. E. 2006. Glacial trinity: Neoproterozoic Earth history within the British–Irish Caledonides. *Geology*, **34**, 909–912.

MCFADDEN, K. A., HUANG, J. *ET AL.* 2008. Pulsed oxidation and biological evolution in Ediacaran Doushantuo Formation. *Proceedings of the National Academy of Sciences (USA)*, **105**, 3197–3202.

MCKIRDY, D. M., BURGESS, J. M. *ET AL.* 2001. A chemostratigraphic overview of the late Cryogenian interglacial sequence in the Adelaide Fold-Thrust Belt, South Australia. *Precambrian Research*, **106**, 149–186.

MELEZHIK, V. A., GOROKHOV, I. M., KUZNETSOV, A. B. & FALLICK, A. E. 2001. Chemostratigraphy of Neoproterozoic carbonates: implications for 'blind dating'. *Terra Nova*, **13**, 1–11.

MELEZHIK, V. A., POKROVSKY, B. G., FALLICK, A. E., KUZNETSOV, A. B. & BUJAKAITE, M. I. 2009. Constraints on the $^{87}Sr/^{86}Sr$ of Late Ediacaran seawater: insights from high-Sr limestones. *Journal of the Geological Society, London*, **166**, 183–191.

MILLER, N. R., STERN, R. J., AVIGAD, D., BEYTH, M. & SCHILMAN, B. 2009. Cryogenian slate-carbonate sequences of the Tambien Group, Northern Ethiopia (I) 'Pre-Sturtian' chemostratigraphy and regional correlations. *Precambrian Research*, **170**, 129–156.

MISI, A. & VEIZER, J. 1998. Neoproterozoic carbonate sequences of the Una Group, Irece Basin, Brazil: chemostratigraphy, age and correlations. *Precambrian Research*, **89**, 87–100.

MISI, A., KAUFMAN, A. J., AZMY, K., DARDENNE, M. A., SIAL, A. N. & DE OLIVEIRA, T. F. 2011. Neoproterozoic successions of the São Francisco Craton, Brazil: The Bambuí, Una, Vazante and Vaza Barris/Miaba groups and their glacigenic deposits. *In*: ARNAUD, E., HALVERSON, G. P. & SHIELDS-ZHOU, G. (eds) *The Geological Record of Neoproterozoic Glaciations*. Geological Society, London, Memoirs, **36**, 509–522.

NAGY, R. M., PORTER, S. M., DEHLER, C. M. & SHEN, Y. 2009. Biotic turnover driven by eutrophication before the Sturtian low-latitude glaciation. *Nature Geoscience*, **2**, 415–418.

NOGUEIRA, A. C. R., RICCOMINI, C., SIAL, A. N., MOURA, C. A. V., TRINDADE, R. I. F. & FAIRCHILD, T. R. 2007. Carbon and strontium isotope fluctuations and paleoceanographic changes in the late Neoproterozoic Araras carbonate platform, southern Amazon craton, Brazil. *Chemical Geology*, **237**, 191–210.

ONO, S., WING, B., JOHNSTON, D., FARQUHAR, J. & RUMBLE, D. 2006. Mass-dependent fractionation of quadruple stable sulfur isotopes as a new tracer of sulfur biogeochemical cycles. *Geochimica et Cosmochimica Acta*, **70**, 2238–2252.

PAVLOV, A. A. & KASTING, J. F. 2002. Mass-independent fractionation of sulfur isotopes in Archean sediments: strong evidence for an anoxic Archean atmosphere. *Astrobiology*, **2**, 27–41.

PAYTAN, A., KASTNER, M., CAMPBELL, D. & THIEMENS, M. H. 1998. Sulfur isotopic composition of Cenozoic seawater sulfate. *Science*, **282**, 1459–1462.

PAYTAN, A., KASTNER, M., CAMPBELL, D. & THIEMENS, M. H. 2004. Seawater sulfur isotopic variations in the Cretaceous. *Science*, **304**, 1663–1665.

PELL, S. D., MCKIRDY, D. M., JANSYN, J. & JENKINS, R. J. F. 1993, Ediacaran carbon isotope stratigraphy of South Australia — an initial study. *Transactions of the Royal Society of South Australia*, **117**, 153–161.

POKROVSKII, B. G., MELEZHIK, V. A. & BUJAKAITE, M. I. 2006. Carbon, oxygen, strontium, and sulfur isotopic compositions in late Precambrian rocks of the Patom Complex, central Siberia: Communication 1. Results, isotope stratigraphy, and dating problems. *Lithology and Mineral Resources*, **41**, 450–474.

POULTON, S. W., FRALICK, P. W. & CANFIELD, D. E. 2004. The transition to a sulphidic ocean ~1.84 billion years ago. *Nature*, **431**, 173–177.

PRAVE, A. R. 1999. Two diamictites, two cap carbonates, two $\delta^{13}C$ excursions, two rifts: The Neoproterozoic Kingston Peak Formation, Death Valley, California. *Geology*, **27**, 339–342.

PRAVE, A. R., FALLICK, A. E., THOMAS, C. W. & GRAHAM, C. M. 2009. A composite C-isotope profile for the Neoproterozoic of Scotland and Ireland. *Journal of the Geological Society, London*, **166**, 845–857.

RAINBIRD, R. H., JEFFERSON, C. W. & YOUNG, G. M. 1996. The early Neoproterozoic sedimentary Succession B of northwestern Laurentia: correlations and paleogeographic significance. *Geological Society of America Bulletin*, **108**, 454–470.

RAISWELL, R., BUCKLEY, F., BERNER, R. A. & ANDERSON, T. F. 1988. Degree of pyritisation of iron as a paleoenvironmental indicator of bottom-water oxygenation. *Journal of Sedimentary Petrology*, **58**, 812–819.

RICE, A. H. N., EDWARDS, M. B., HANSEN, T. A., ARNAUD, E. & HALVERSON, G. P. 2011. Glaciogenic rocks of the Neoproterozoic Smalfjord and Mortensnes Formations, Vestertana Group, E. Finnmark, Norway. *In*: ARNAUD, E., HALVERSON, G. P. & SHIELDS-ZHOU, G. (eds) *The Geological Record of Neoproterozoic Glaciations.* Geological Society, London, Memoirs, **36**, 593–602.

RIES, J. B., FIKE, D. A., PRATT, L. M., LYONS, T. W. & GROTZINGER, J. P. 2009. Superheavy pyrite ($\delta^{34}S_{pyr} > \delta^{34}S_{CAS}$) in the terminal Proterozoic Nama Group, southern Namibia: a consequence of low seawater sulfate at the dawn of animal life. *Geology*, **37**, 743–746.

ROONEY, A. D., SELBY, D., HOUZAIT, J.-P. & RENNE, P. R. 2010. Re–Os geochronology of a Mesoproterozoic sedimentary succession, Taoudeni basin, Mauritania: Implications for basin-wide correlations and Re–Os organic-rich sediments systematic. *Earth and Planetary Science Letters*, **289**, 486–496.

ROSE, C. V. & MALOOF, A. C. 2010. Testing models for post-glacial "cap dolostone" deposition: Nuccaleena Formation, South Australia. *Earth and Planetary Science Letters*, **296**, 165–180.

ROTHMAN, D. H., HAYES, J. M. & SUMMONS, R. E. 2003. Dynamics of the Neoproterozoic carbon cycle. *Proceedings of the National Academy of Sciences (USA)*, **100**, 124–129.

SAWAKI, Y., KAWAI, T. *ET AL.* 2010*a*. $^{87}Sr/^{86}Sr$ chemostratigraphy of Neoproterozoic Dalradian carbonates below the Port Askaig glaciogenic Formation, Scotland. *Precambrian Research*, **179**, 150–164.

SAWAKI, Y., OHNO, T. *ET AL.* 2010*b*. The Ediacaran radiogenic Sr isotope excursion in the Doushantuo Formation in the Three Gorges area, South China. *Precambrian Research*, **176**, 46–64.

SAYLOR, B. Z., KAUFMAN, A. J., GROTZINGER, J. P. & URBAN, F. 1998. A composite reference section for Terminal Proterozoic strata of southern Namibia. *Journal of Sedimentary Research*, **68**, 1223–1235.

SCHRAG, D. P., BERNER, R. A., HOFFMAN, P. F. & HALVERSON, G. P. 2002. On the initiation of a snowball Earth. *Geochemistry, Geophysics, Geosystems*, **31**, doi: 10.1029/2001GC000219.

SCHIDLOWSKI, M., EICHMANN, R. & JUNGE, C. E. 1975. Precambrian sedimentary carbonates: carbon and oxygen isotope geochemistry

and implications for the terrestrial oxygen budget. *Precambrian Research*, **2**, 1–69.

Schröder, S., Schreiber, C., Amthor, J. E. & Matter, A. 2004. Stratigraphy and environmental conditions of the terminal Neoproterozoic–Cambrian Period in Oman: evidence from sulphur isotopes. *Journal of the Geological Society, London*, **161**, 489–499.

Shen, B., Xiao, S., Zhou, C., Kaufman, A. J. & Yuan, X. 2010. Carbon and sulfur isotope chemostratigraphy of the Neoproterozoic Quanji Group of the Chaidam Basin, NW China: Basin stratification in the aftermath of an Ediacaran glaciation post-dating the Shuram event? *Precambrian Research*, **177**, 241–252.

Shields, G. A. 1999. Working towards a new stratigraphic calibration scheme for the Neoproterozoic–Cambrian. *Eclogae Geologicae Helvetiae*, **92**, 221–233.

Shields, G. A. 2005. Neoproterozoic cap carbonates: a critical appraisal of existing models and the plumeworld hypothesis. *Terra Nova*, **17**, 299–310.

Shields, G. A. 2007. A normalised seawater strontium isotope curve: possible implications for Neoproterozoic–Cambrian weathering rates and further oxygenation of the Earth. *Earth*, **2**, 35–42.

Shields, G. & Veizer, J. 2002. Precambrian marine carbonate isotope database: Version 1.1. *Geochemistry, Geophysics, Geosystems*, **3**, doi: 10.1029/2001GC000266.

Shields, G., Stille, P., Brasier, M. D. & Atudorei, N.-V. 1997. Stratified oceans and oxygenation of the late Precambrian environments: a post glacial geochemical record from the Neoproterozoic. *Terra Nova*, **9**, 218–222.

Shields, G. A., Strauss, H., Howe, S. S. & Siegmund, H. 1999. Sulphur isotope compositions of sedimentary phosphorites from the basal Cambrian of China — implications for Neoproterozoic–Cambrian biogeochemical cycling. *Journal of the Geological Society, London*, **156**, 943–957.

Shields, G., Kimura, H., Yang, J. & Gammon, P. 2004. Sulphur isotopic evolution of Neoproterozoic–Cambrian seawater: new francolite-bound sulphate S data and critical appraisal of the existing record. *Chemical Geology*, **204**, 163–182.

Sial, A. N., Dardenne, M. A. *et al*. 2010. The São Francisco Paleocontinent. *In*: Gaucher, C., Sial, A. N., Halverson, G. P. & Frimmel, H. (eds) *Neoproterozoic–Cambrian Tectonics, Global Change and Evolution: A focus on Southwestern Gondwana*. Developments in Precambrian Geology, Elsevier, Dordrecht, **16**, 31–69.

Strauss, H. 1993. The sulfur isotopic record of Precambrian sulfates: new data and a critical evaluation of the existing record. *Precambrian Research*, **63**, 225–246.

Swanson-Hysell, N. L., Rose, C. V., Calmet, C., Halverson, G. P., Hurtgen, M. T. & Maloof, A. C. 2010. Cryogenian glaciation and onset of carbon-isotope decoupling. *Science*, **328**, 608–611.

Tucker, M. E. 1986. Carbon isotope excursions in Precambrian/Cambrian boundary beds. *Nature*, **319**, 48–50.

Turner, E. C. 2009. Lithostratigraphy and stable isotope values of the early Neoproterozoic Gypsum Formation (Little Dal Group), Mackenzie Mountains Supergroup, NWT. *NWT Open Report*, 2009-002.

Veizer, J., Compston, W., Clauer, N. & Schidlowski, M. 1983. $^{87}Sr/^{86}Sr$ in late Proterozoic carbonates: evidence for a 'mantle' event at ~900 Ma. *Geochimica et Cosmochimica Acta*, **47**, 295–302.

Walter, M. R., Veevers, J. J., Calver, C. R., Gorjan, P. & Hill, A. C. 2000. Dating the 840–544 Ma Neoproterozoic interval by isotopes of strontium, carbon, and sulfur in seawater and some interpretive models. *Precambrian Research*, **100**, 371–433.

Williams, G. E. 1979. Sedimentology, stable-isotope geochemistry and palaeoenvironment of dolostones capping late Precambrian glacial sequences in Australia. *Journal of the Geological Society of Australia*, **26**, 377–386.

Workman, R. K., Grotzinger, J. P. & Hart, S. R. 2002. Constraints on Neoproterozoic ocean chemistry from C and B analyses of carbonates from the Witvlei and Nama groups, Namibia. *In*: *Goldschmidt Conference Proceedings* (Davos, Switzerland).

Xiao, S., Bao, H. *et al*. 2004. The Neoproterozoic Quruqtagh Group in eastern Chinese Tianshan: evidence for a post-Marinoan glaciation. *Precambrian Research*, **130**, 1–26.

Xu, B., Xiao, S. *et al*. 2009. SHRIMP zircon U–Pb age constraints on Neoproterozoic Quruqtagh diamictites in NW China. *Precambrian Research*, **168**, 247–258.

Yoshioka, H., Asahara, Y., Tojo, B. & Kawakami, S. 2003. Systematic variations in C, O, and Sr isotopes and elemental concentrations in Neoproterozoic carbonates in Namibia: implications for glacial to interglacial transition. *Precambrian Research*, **124**, 69–85.